AD-A230 473

ᴵᴿᴱᴬᴸᴵˢᵀᴵᶜ ᴼᴿᴮᴵᵀˢ

ABOUT THE MARTIAN MOONS

THESIS

Samuel R. Bryant
Captain. USAF

AFIT/GA/ENY/90D-1

DEPARTMENT OF THE AIR FORCE
AIR UNIVERSITY

AIR FORCE INSTITUTE OF TECHNOLOGY

Wright-Patterson Air Force Base, Ohio

91 1 3 095

REALISTIC ORBITS

ABOUT THE MARTIAN MOONS

THESIS

Samuel R. Bryant
Captain, USAF

AFIT/GA/ENY/90D-1

AFIT/GA/ENY/90D-1

REALISTIC ORBITS

ABOUT THE MARTIAN MOONS

THESIS

Presented to the Faculty of the School of Engineering

of the Air Force Institute of Technology

Air University

In Partial Fulfillment of the

Requirements for the Degree of

Master of Science in Astronautical Engineering

Samuel R. Bryant, B.S.

Captain, USAF

December, 1990

Acknowledgements

Upon completion of my thesis, I would like to express my gratitude to Dr. William Wiesel, my thesis advisor, for his patience and expert guidance during my research. His support made this project both educational and interesting.

I would also like to sincerely thank my wife and dearest friend Darcy, who worked as hard as I did to maintain our sanity as well as the household and Sarah while I was locked in the computer room or lost in the halls of the library. Her efforts and support made my research go that much farther.

Accession For		
NTIS GRA&I	☒	
DTIC TAB	☐	
Unannounced	☐	
Justification		
By		
Distribution/		
Availability Codes		
Dist	Avail and/or Special	
A-1		

Table of Contents

List of Figures

List of Tables

Notation

a	semi-major axis of the moon
dM	differential element of mass
$\vec{d}$	position vector of satellite with respect to Mars
$\vec{D}$	position vector of the moon with respect to Mars
e	eccentricity of the moon
GM	gravitational parameter
H	Hamiltonian
I_{XX}, I_{YY}, I_{ZZ}	moon mass moments of inertia
I_{XY}, I_{XZ}, I_{YZ}	moon mass products of inertia
L	Lagrangian
m_{sat}	mass of satellite
M	mean anomaly
P_i	generalized momenta
Q_i	generalized coordinates
$\dot{r}$	position vector of the satellite with respect to a differential element of moon mass
$\vec{R}$	position vector of the satellite with respect to the moon
T	kinetic energy

v	velocity
V	potential energy
x	minimum axis of inertia of the moon
y	intermediate axis of inertia of the moon
z	maximum axis of inertia of the moon
$\vec{\beta}$	position vector of differential element of moon mass with respect to the moon's center of gravity
Ω	angular velocity - rotation rate of the moon
ω	angular velocity - revolution rate of the moon
ν	true anomaly

Abstract

Orbits about the Martian moons, Phobos and Deimos, previously found to be stable by the Poincaré surface of section technique in a restricted three-body system, were investigated with non-zero eccentricity of the moons added to the dynamics. Hamilton's canonical equations were derived to describe the dynamics of the planar four body system (Mars, moon, sun, artificial satellite). Although not strictly applicable to this case, the surface of section technique was used to verify whether or not the previously found stable orbits were realistic when a real world perturbation was added to the system dynamics. The surface of section technique involves the numerical integration of several orbits with the same initial value of the Hamiltonian based on matching the angular rates of the orbit and the moon with respect to Mars. Apoapsis and periapsis points of the orbits were plotted in the two-dimensional configuration space. Stable orbits were found when the points form regions which are bounded; chaotic orbits were indicated by random points.

REALISTIC ORBITS
ABOUT THE MARTIAN MOONS

I. Introduction

A future manned mission to Mars will be a historic achievement, and the possible advancements in scientific knowledge of the solar system are unimaginable. However, when the overall cost of such a venture is considered, space exploration is also astronomically expensive.

A manned mission to Mars will require extensive life support equipment, supplies, and repair materials. Basic supplies such as water, oxygen, and food must be stored in the spacecraft with the astronauts during the entire length of the mission. Life support equipment or the vehicle structure may need repair during the mission which necessitates carrying along tools and raw materials. These items must also be stored on the spacecraft. All this extra weight translates directly into additional cost (in energy) to launch the spacecraft from earth.

Due to the earth's strong gravitational field, any extra weight is very expensive in terms of the amount of energy (rocket thrust) needed to escape the earth's gravity and enter orbit. If earth's gravitational field were half as strong there would be a significant savings in energy that could be used elsewhere in the mission planning, such as mission duration

1

or final destination.

Since it is not possible to change the earth's gravitational field, one logical solution is to find a small moon or asteroid that can act as a way-station or refueling stop. This way-station will have a smaller gravitational field than the earth's so spacecraft will use much less energy to land and take off. While on the way-station, astronauts could mine the surface for needed materials, minerals, and water which would save precious energy and extend the overall duration of the mission.

For a manned mission to Mars, the logical choice for a way-station is one of its small moons. Phobos is the more interesting and useful choice due to its larger size and closer proximity to Mars. Both moons are believed to be asteroids that were captured by Mars' gravitational field. However, their extremely small size and close proximity to Mars means that any orbit around either moon will be greatly influenced by the gravity of Mars (1:18). The question then becomes one of stability of the orbit.

When the Russians launched the Phobos 2 scientific probe in July 1988, it was the first Mars mission since the two U.S. Viking probes were launched in 1975 (2:42). The data from the Phobos 2 probe answered many questions about Mars and its two moons. The probe's unfortunate computer failure in March 1989 did not diminish the success of its 57 days in orbit around Mars and Phobos (3:156).

Updated orbital parameters of Phobos will allow accurate predictions of the moon's location. This new data reduces the uncertainty of the moon's position from 500 kilometers (km) to 4 km (2:46). Since the diameter of Phobos is only 27 km on its longest axis (1:19), a 500 km error in predict-

2

ing its current position prevented any previous rendezvous or landing attempt. A 4 km error in position can easily be handled by the spacecraft's computer and guidance system.

The gravitational field of Phobos was accurately determined before the Phobos 2 probe failed. Escape velocity (speed needed to escape local gravity) for Phobos is 8 miles per hour (mph) (1:18). Earth's escape velocity is 25,000 mph and requires an enormous amount of highly-explosive fuel (1:17-18). The much smaller gravitational field on Phobos is a major reason for selecting it as a possible future way-station.

Phobos 2 did return some disappointing data about the amount of water on the surface of Phobos. Although many scientists want to believe Phobos is an oasis for future colonies on Mars, the Infrared Spectrometer (ISM) experiment found an extremely low amount of hydration in the first five meters of the surface (3:158-159) indicating much less hydration in the regolith (fractured surface layer) than on most known asteroids and less than what has been found on the surface of Mars (3:159). This does not eliminate the possibility that water may be found deeper than the regolith. Even if Phobos is completely dry, it is still an excellent choice for continuing scientific research of the sun's gamma rays and the gravitational and magnetic fields of Mars.

II. Approach/Methodology

Previous work by Jansson (4) proved that stable orbits about the Martian moons are possible, but the use of several simplifying assumptions listed below may make the orbits unrealistic:

Phobos and Deimos have circular orbits about Mars.

Mars is treated as a point mass.

The sun's gravity field is ignored.

Combining these assumptions may have over-simplified the problem and produced unrealistic solutions. This research will analyze the stable orbits around Phobos and Deimos found by Jansson to see if the orbits remain stable after including realistic perturbation terms in the analysis.

Stable orbits around the Martian moons will be investigated using the Poincaré surface of section stability technique. The equations of motion will be derived using the Hamiltonian of the four body problem (Mars, moon, spacecraft, sun). Since this system is not a conservative two degree-of-freedom Hamiltonian system, the surface of section technique is not strictly applicable. The surface of section stability technique numerically integrates the parameters of several test orbits using the same Hamiltonian value. These test orbits will be numerically integrated in four-dimensional space and then plotted in two-dimensional space. Each dot on the plot will represent a closest (periapsis) or farthest (apoapsis) point in the orbit. New dots for each orbit will represent a small perturbation (change) in the orbit. If the dots produce a closed circle or ellipse, the orbit is bounded and therefore stable. Random or chaotic patterns will indicate unstable

4

orbits. Plots will be made of each trajectory to see if the orbit remains stable as realistic perturbations are added to the system dynamics.

III. Problem Dynamics

The coordinate system used is illustrated in Figure 1 showing the moon modeled as a triaxial ellipsoid with an exaggerated misalignment of the x axis due to the eccentricity of the moon.

Jansson's research assumed the moons' orbits around Mars were circular (eccentricity = 0). Although the eccentricities of Phobos and Deimos are small (.015 and .00052 respectively) (4:2), this investigation will not assume circular orbits in order to achieve realistic results. Since the orbits will not be circular, the constant rotation rates (Ω) of the moons about their z axis will not be equal to their non-constant revolution rates (ω) about Mars. This makes the dynamics more complicated because the moon's minimum axis of inertia (x) will not remain pointed toward Mars while the moon rotates about its maximum axis of inertia (z). The intermediate axis of inertia (y) completes the orthogonal set of axes.

Also, if the orbits about Phobos continue to remain stable, the J_2 term of the geopotential of Mars will be included. This investigation will also consider the sun's gravitational attraction modeled as a point mass due to its distance from the satellite.

Equations of Motion

The equations of motion of the satellite can be derived in the form of the Hamilton's canonical equations. The Hamiltonian is defined as

$$H = \sum P_i \dot{Q}_i - L \qquad (1)$$

6
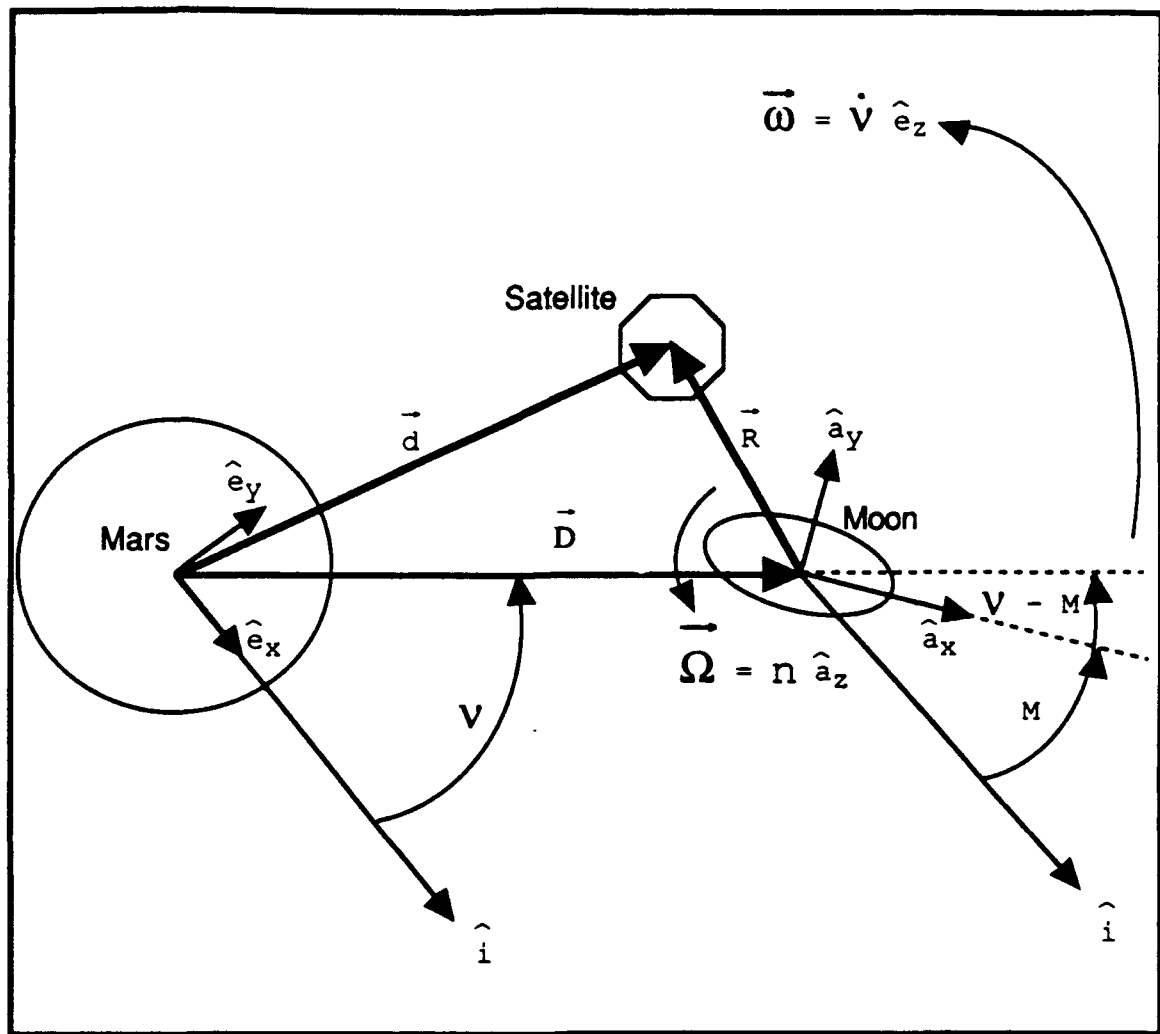
Figure 1. Coordinate System

7

where P_i and Q_i are the generalized momenta and generalized coordinates, respectively. L is defined as the Lagrangian and is found by

$$L = T - V \tag{2}$$

where T and V are the kinetic energy and potential energy, respectively. The first step in deriving the equations of motion is to define T and V of the system in terms of the generalized coordinates (Q_i's) and generalized velocities ($\dot{Q}_i$'s).

Kinetic Energy. The kinetic energy of the satellite as it orbits about the Martian moon is given by

$$T_{sat} = \frac{1}{2} m v^2 \tag{3}$$

where m is the mass of the satellite and v is the inertial velocity of the satellite. Based on very small moon masses, the the inertial reference frame is set at the mass center of Mars.

Now

$$\vec{v} = \dot{\vec{d}} \tag{4}$$

where a dot over a vector represents the time rate of change of the vector with respect to the inertial frame (inertial derivative).

8

Therefore,

$$v^2 = \dot{\vec{d}} \cdot \dot{\vec{d}} \tag{5}$$

and from Figure 1

$$\vec{d} = \vec{D} + \vec{R} \tag{6}$$

leading directly to

$$\dot{\vec{d}} = \dot{\vec{D}} + \dot{\vec{R}} \tag{7}$$

Here, $\dot{\vec{R}}$ may be written as

$$^i\frac{d}{dt}\vec{R} = {}^r\frac{d}{dt}\vec{R} + \left(\vec{\omega}^{\,ri} \times \vec{R}\right) \tag{8}$$

where the superscripts i and r indicate derivatives taken in the inertial and rotating (moon-fixed) frames, respectively, with the moon rotating at a fixed rate.

From Figure 1,

$$\vec{\omega}^{\,ri} = \vec{\Omega} = \Omega\,\hat{a}_z \tag{9}$$

and

$$\vec{R} = X\,\hat{a}_x + Y\,\hat{a}_y + Z\,\hat{a}_z \tag{10}$$

9

which yields

$$\dot{\vec{R}} = \dot{X}\,\hat{a}_x + \dot{Y}\,\hat{a}_y + \dot{Z}\,\hat{a}_z + \left[\left(\Omega\,\hat{a}_z\right) \times \left(X\,\hat{a}_x + Y\,\hat{a}_y + Z\,\hat{a}_z\right)\right] \qquad (11)$$

and simplifies to

$$\dot{\vec{R}} = \left(\dot{X} - \Omega Y\right)\hat{a}_x + \left(\dot{Y} + \Omega X\right)\hat{a}_y + \dot{Z}\,\hat{a}_z. \qquad (12)$$

Since we are not assuming the moon is in a circular orbit about Mars, the $\vec{D}$ term becomes complicated because the moon's X axis does not remain fixed on the mass center of Mars as the moon revolves around Mars. Taking this into account, the magnitude of $\vec{D}$ will not remain constant and will be calculated by (5:76)

$$D = \frac{a\left(1 - e^2\right)}{1 + e\cos v} \qquad (13)$$

where the true anomaly, v, is defined as the angle from the moon's closest approach (perimartem) to the current position vector $\vec{D}$. The mean anomaly (M) is the mean motion (n) of the moon multiplied by the time since perimartem passage. The difference between the moon's x axis and $\vec{D}$ from the mass center of Mars is the difference between v and M. This is sometimes called the "equation of center" (5:77) and is shown in Figure 1 as $v - M$. The letters a and e refer to the moon's orbital semi-major axis and eccentricity, respectively.

Approximating equation (13) by a periodic expansion in e and dis-

carding fourth order terms and higher (5:76), because their contribution is negligible (< .5 km), yields

$$D \approx a \left(1 + \frac{1}{2} e^2 - e \cos M - \frac{1}{2} e^2 \cos 2M + \frac{3}{8} e^3 \cos M \right.$$

$$\left. - \frac{3}{8} e^3 \cos 3M + \cdots \right) \tag{14}$$

Similarly, the "equation of center", defined as $v - M$, can be approximated by (5:77)

$$(v - M) \approx \left(2e - \frac{1}{4} e^3 \right) \sin M + \frac{5}{4} e^2 \sin 2M + \frac{13}{12} e^3 \sin 3M + \cdots \tag{15}$$

The position vector $\vec{D}$ can now be written as

$$\vec{D} = D \cos(v - M) \, \hat{a}_x - D \sin(v - M) \, \hat{a}_y. \tag{16}$$

As in equation (8), $\dot{\vec{D}}$ can be written as

$$\frac{{}^i d}{dt} \vec{D} = \frac{{}^r d}{dt} \vec{D} + \left(\vec{\omega}^{ri} \times \vec{D} \right). \tag{17}$$

The first term on the right hand side of equation (17) is written as

$$\frac{{}^r d}{dt} \vec{D} = \frac{{}^r d}{dt} \left[D \cos (v - M) \right] \hat{a}_x - \frac{{}^r d}{dt} \left[D \sin (v - M) \right] \hat{a}_y \tag{18}$$

11

and the product rule yields

$$r\frac{d}{dt}\vec{D} = \left[D' \cos(v - M) - D(v - M)' \sin(v - M)\right]\hat{a}_x$$
$$- \left[D' \sin(v - M) + D(v - M)' \cos(v - M)\right]\hat{a}_y \qquad (19)$$

where

$$D' = a\Omega\left(e \sin M + e^2 \sin 2M - \frac{3}{8} e^3 \sin M + \frac{9}{8} e^3 \sin 3M\right) \qquad (20)$$

and

$$(v - M)' = \Omega\left[\left(2e - \frac{1}{4} e^3\right) \cos M + \frac{5}{2} e^2 \cos 2M + \frac{13}{4} e^3 \cos 3M\right]. \qquad (21)$$

The second term on the right hand side of equation (17) is not as complicated and is written as

$$\vec{\omega}^{ri} \times \vec{D} = \Omega\, \hat{a}_z \times \left(D \cos(v - M)\, \hat{a}_x - D \sin(v - M)\, \hat{a}_y\right) \qquad (22)$$

and yields

$$\vec{\omega}^{ri} \times \vec{D} = \Omega D\left[\sin(v - M)\, \hat{a}_x + \cos(v - M)\, \hat{a}_y\right] \qquad (23)$$

1 2

Combining equations (19) and (23) and then simplifying results in

$$\dot{\vec{D}} = \left[D'\cos(v - M) + D\sin(v - M)\left\{ \Omega - (v - M)' \right\} \right]\hat{a}_x$$
$$+ \left[D\cos(v - M)\left\{ \Omega - (v - M)' \right\} - D'\sin(v - M) \right]\hat{a}_y. \tag{24}$$

Combining equations (12) and (24) into equation (7) gives

$$\dot{\vec{d}} = \left[\dot{X} - \Omega Y + D'\cos(v - M) + D\sin(v - M)\left\{ \Omega - (v - M)' \right\} \right]\hat{a}_x$$
$$+ \left[\dot{Y} + \Omega X + D\cos(v - M)\left\{ \Omega - (v - M)' \right\} - D'\sin(v - M) \right]\hat{a}_y$$
$$+ \dot{Z}\,\hat{a}_z \tag{25}$$

Since the dynamics are assumed to remain in the same plane of motion, the Z term will be set to zero so the surface of section technique can be used.

Finally, combining equations (25), (5), and (3) gives the total kinetic energy of the satellite as

$$T_{sat} = \frac{1}{2}m_{sat}\left[\dot{X} - \Omega Y + D'\cos(v - M) + D\sin(v - M)\left(\Omega - (v - M)' \right) \right]^2$$
$$+ \frac{1}{2}m_{sat}\left[\dot{Y} + \Omega X + D\cos(v - M)\left(\Omega - (v - M)' \right) - D'\sin(v - M) \right]^2 \tag{26}$$

<u>Potential Energy</u>. The potential energy of the satellite can be divided into three parts

$$V_{sat} = V_{moon} + V_{Mars} + V_{sun} \tag{27}$$

1 3

<u>Potential Energy Due to the Moon</u>. The potential energy of the satellite due to the gravitational attraction of the moon is not simple due to the non-spherical shape of the moon. The moon can be modeled as a tri-axial ellipsoid as shown in Figure 2. The gravitational potential for an arbitrarily shaped body is given by Meirovitch (6:430-436) starting with the integral form of the inverse square force field formula

$$V_{moon} = -Gm_{sat} \int \frac{dM_{moon}}{r}$$
(28)

where G is the universal gravitational constant and from Figure 2

$$r = |\vec{r}| = |\vec{R} + \vec{\beta}|$$
(29)

$$\vec{\beta} = a\,\hat{a}_x + b\,\hat{a}_y + c\,\hat{a}_z$$
(30)

$$\beta^2 = a^2 + b^2 + c^2$$
(31)

$$R^2 = X^2 + Y^2 + Z^2$$
(32)

$$\vec{R} \cdot \vec{\beta} = aX + bY + cZ$$
(33)

Now equation (29) can be moved to the numerator and written as

$$r^{-1} = |\vec{R} - \vec{\beta}|^{-1} = [(\vec{R} - \vec{\beta})^2]^{-1/2}$$
(34)

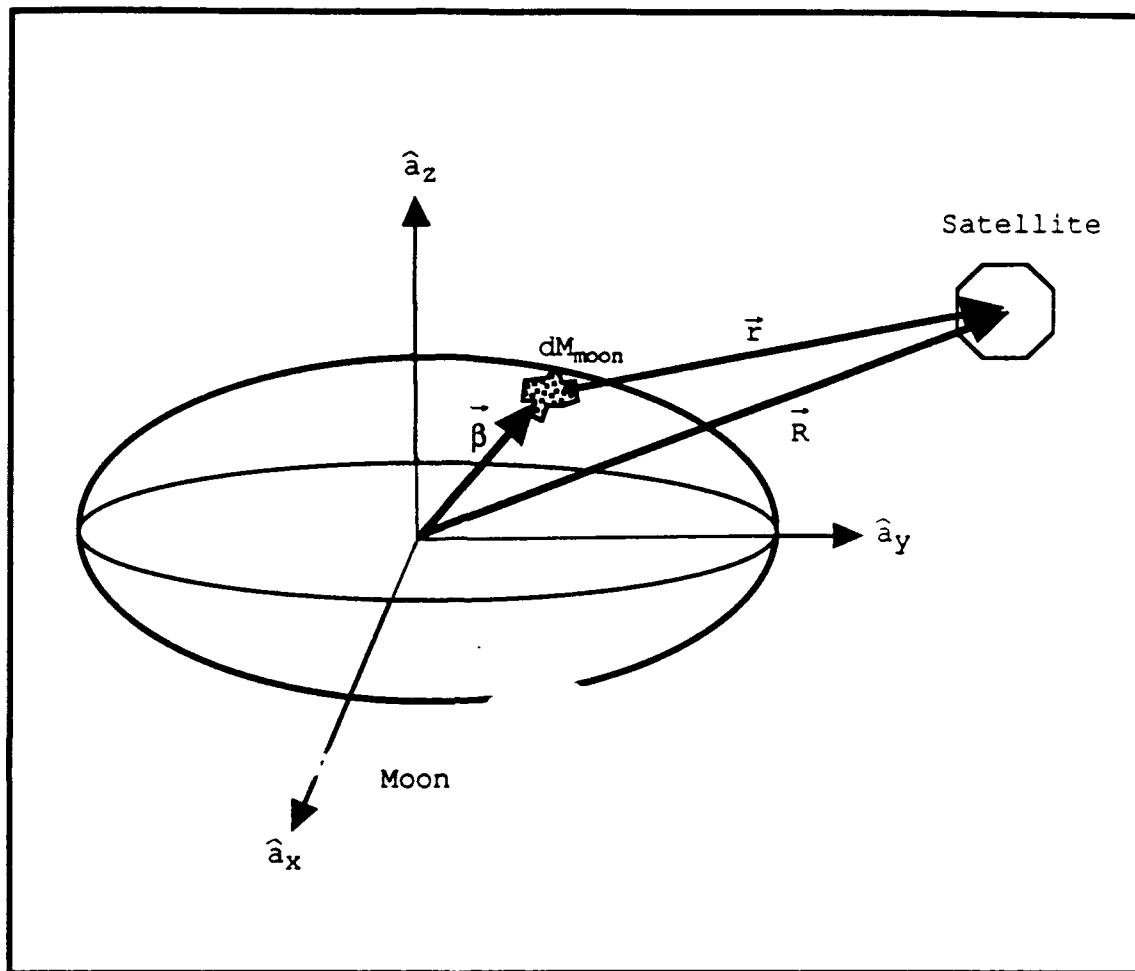$$r^{-1} = (R^2 - 2\vec{R} \cdot \vec{\beta} + \beta^2)^{-1/2}$$
(35)

1 4

Figure 2. Gravitational Potential Due to Moon

1 5

$$r^{-1} = \left[R^2 \left(1 - \frac{2\vec{R} \cdot \vec{\beta}}{R^2} + \frac{\beta^2}{R^2} \right) \right]^{-1/2} \tag{36}$$

$$r^{-1} = R^{-1} \left[\left(1 - \frac{2\vec{R} \cdot \vec{\beta}}{R^2} + \frac{\beta^2}{R^2} \right) \right]^{-1/2} \tag{37}$$

Using a binomial expansion and ignoring terms higher than second order because their contribution is negligible ($< .5$ km), equation (37) can be written in the form of a power series as

$$r^{-1} = R^{-1} \left[1 + \frac{\vec{R} \cdot \vec{b}}{R^2} - \frac{1}{2}\left(\frac{\beta}{R}\right)^2 + \frac{3}{8}\left(\frac{2\vec{R} \cdot \vec{b}}{R^2} - \left(\frac{\beta}{R}\right)^2 \right)^2 + \cdots \right] \tag{38}$$

$$r^{-1} = R^{-1} + R^{-3}\left(\vec{R} \cdot \vec{\beta} \right) - \frac{1}{2}R^{-3}\beta^2 + \frac{3}{2}R^{-5}\left(\vec{R} \cdot \vec{\beta} \right)^2 + \cdots \tag{39}$$

Combining equations (28), (31)-(33) and (39) yields

$$V_{moon} = - \frac{Gm_{sat}}{R} \int dM_{moon} - \frac{Gm_{sat}}{R^3} \int (aX + bY + cZ)\, dM_{moon}$$

$$+ \frac{Gm_{sat}}{2R^3} \int (a^2 + b^2 + c^2)\, dM_{moon}$$

$$- \frac{3Gm_{sat}}{2R^5} \int (aX + bY + cZ)^2\, dM_{moon} \quad . \tag{40}$$

Integrating the first term of equation (40) is trivial and the second term vanishes because the origin is taken to be at the center of mass leaving the last two terms which can be combined as

$$-\frac{Gm_{sat}}{2R^3} \int \left[3R^{-2}(aX + bY + cZ)^2 - (a^2+b^2+c^2)\right] dM_{moon}$$

(41)

or

$$\frac{-Gm_{sat}}{2R^3}\left[\begin{array}{c} (3R^{-2}X^2 - 1)\int a^2 dM_{moon} + (3R^{-2}Y^2 - 1)\int b^2 dM_{moon} \\ +(3R^{-2}Z^2 - 1)\int c^2 dM_{moon} \\ + 6R^{-2}\left(XY\int abdM_{moon} + XZ\int acdM_{moon} + YZ\int bcdM_{moon}\right) \end{array}\right]$$

(42)

Defining the mass moments and mass products of inertia from Likens (7:525), it follows from Meirovitch (6:435) that

$$\int a^2 \, dM_{moon} = \frac{1}{2}(I_{zz} + I_{yy} - I_{xx})$$

(43)

$$\int b^2 \, dM_{moon} = \frac{1}{2}(I_{zz} + I_{xx} - I_{yy})$$

(44)

$$\int c^2 \, dM_{moon} = \frac{1}{2}(I_{xx} + I_{yy} - I_{zz})$$

(45)

$$\int ab \, dM_{moon} = I_{xy}$$

(46)

$$\int ac \, dM_{moon} = I_{xz}$$

(47)

$$\int bc \, dM_{moon} = I_{yz}$$

(48)

using the principal axes frame, we have

$$I_{xy} = I_{xz} = I_{yz} = 0.$$

(49)

This simplifies equation (42) allowing the total potential energy of the satellite due to the moon to be written as

$$V_{moon} = -\frac{Gm_{sat}M_{moon}}{R} + \frac{Gm_{sat}}{4R^3}(I_{xx} + I_{yy} + I_{zz})$$

$$-\frac{3Gm_{sat}}{4R^5}\left[X^2(I_{yy} + I_{zz} - I_{xx})\right]$$

$$-\frac{3Gm_{sat}}{4R^5}\left[Y^2(I_{xx} + I_{zz} - I_{yy})\right]$$

$$-\frac{3Gm_{sat}}{4R^5}\left[Z^2(I_{xx} + I_{yy} - I_{zz})\right]$$

(50)

Potential Energy Due to Mars. The potential energy of the satellite due to the gravitational attraction of Mars is the Newtonian term plus the J_2 term of the geopotential simplified due to the planar restrictions.

$$V_{Mars} = - \frac{Gm_{sat}M_{Mars}}{d}\left[1 + \frac{J_2}{2}\left(\frac{R_{Mars}}{d}\right)^2\right]$$

(51)

Now d is defined as

$$d = |\vec{d}| = |\vec{D} + \vec{R}|$$

(52)

and $\vec{D}$ and $\vec{R}$ are defined by equations (10) and (16) respectively and yield

$$d = \left|\left[X + D\cos(v - M)\right]\hat{a}_x + \left[Y - D\sin(v - M)\right]\hat{a}_y\right|$$

(53)

$$d = \sqrt{\left[X + D\cos(v - M)\right]^2 + \left[Y - D\sin(v - M)\right]^2}$$

(54)

Potential Energy Due to the Sun. The potential energy of the satellite due to the gravitational attraction of the sun can be treated as a third body perturbation (8:89-95). The disturbing function for general third body perturbations can be determined from Figure 3 and is written as

$$V_j = - Gm_{sat}\,M_j\left(\frac{1}{\rho_{2j}} - \frac{\vec{\rho}_j \cdot \vec{\rho}}{\rho_j^3}\right)$$
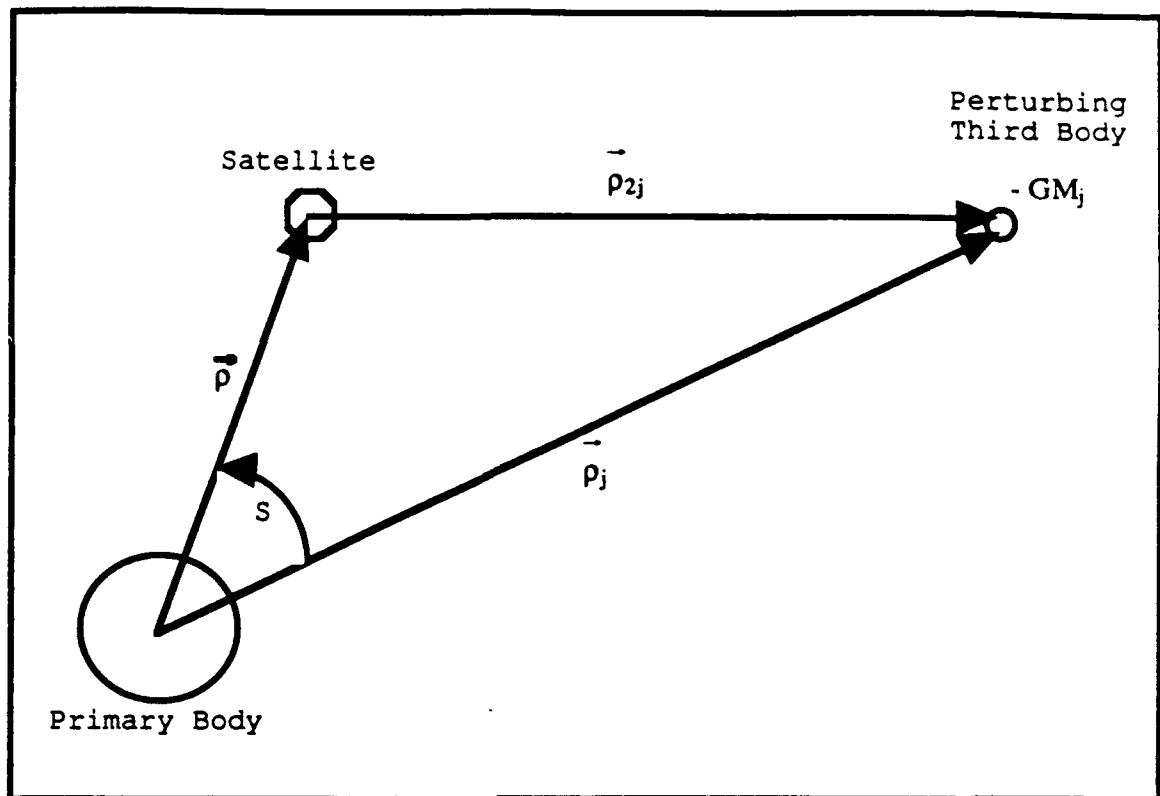
(55)

19

Figure 3. Coordinate System for General Third Body
Disturbing Function

20

For the sun-Mars-satellite system it may be written as

$$V_{sun} = -Gm_{sat}M_{sun}\left(\frac{1}{\rho_{2sun}} - \frac{\vec{\rho}_{sun} \cdot \vec{d}}{\rho_{sun}^3}\right)$$

(56)

where $\vec{\rho}_{2sun}$ is the vector from the satellite to the perturbing mass (the sun) and $\vec{\rho}_{sun}$ locates the third mass relative to the primary body (Mars). The first term on the right hand side of equation (56) is called the direct term and represents the direct gravitational attraction of the third mass on the satellite. The second term on the right hand side of equation (56) is the indirect term and represents perturbations of the third mass on the primary body.

Now the indirect term can be written as

$$V_{indirect} = Gm_{sat}M_{sun}\left(\frac{\vec{\rho}_{sun} \cdot \vec{d}}{\rho_{sun}^3}\right) = GM_{sun}\left(\frac{d}{\rho_{sun}^2}\right)\cos S$$

(57)

and the direct term becomes

$$V_{direct} = -\frac{Gm_{sat}M_{sun}}{\rho_{2sun}} = -\frac{Gm_{sat}M_{sun}}{\rho_{sun}}\left(1 - 2\alpha\cos S + \alpha^2\right)^{-1/2}$$

(58)

letting

$$\alpha = \frac{d}{\rho_{sun}}$$

(58.1)

21

If the ratio α is quite small (as it is in this case), a direct expansion in powers of α will be rapidly convergent. This approach is called the Lunar Theory (8:91) and allows a binomial expansion of equation (58) which yields

$$V_{direct} = -\frac{Gm_{sat}M_{sun}}{\rho_{sun}}\left[1 + \alpha\cos S + \alpha^2\left(-\frac{1}{2} + \frac{3}{2}(\cos S)^2\right) + \cdots\right]$$

(59)

The first term in this expansion does not contain the coordinates of the satellite and therefore can be ignored. The second term exactly cancels the $V_{indirect}$ term leaving

$$V_{sun} = -\frac{Gm_{sat}M_{sun}d^2}{2\rho_{sun}^3}(3(\cos S)^2 - 1)$$

(60)

where $(\cos S)$ can be written as

$$\cos S = \frac{\overline{\rho_{sun}} \cdot \overline{R}}{|\overline{\rho_{sun}}| \, |\overline{R}|}$$

(60.1)

with $\overline{R}$ defined by equation (10) and $\overline{\rho_{sun}}$ will be approximated by

$$\overline{\rho}_{sun} = \rho_{sun}\cos M \,\hat{a}_x - \rho_{sun}\sin M \,\hat{a}_y$$

(60.2)

22

Finally, equation (27) can now be written as

$$
\begin{aligned}
V_{sat} = {} & - \frac{Gm_{sat}M_{moon}}{R} + \frac{Gm_{sat}}{4R^3}(I_{xx} + I_{yy} + I_{zz}) \\
& - \frac{3Gm_{sat}}{4R^5}\left[X^2(I_{yy} + I_{zz} - I_{xx})\right] \\
& - \frac{3Gm_{sat}}{4R^5}\left[Y^2(I_{xx} + I_{zz} - I_{yy})\right] \\
& - \frac{Gm_{sat}M_{Mars}}{d}\left[1 + \frac{J_2}{2}\left(\frac{R_{Mars}}{d}\right)^2\right] \\
& - \frac{Gm_{sat}M_{sun}d^2}{2\rho_{sun}^3}\left(3(\cos S)^2 - 1\right)
\end{aligned}
\tag{61}
$$

Lagrangian. The Lagrangian is now needed and is formed by combining equations (2), (26), and (61). Dividing out the mass of the satellite allows the Lagrangian to be written in a per unit mass basis as

$$
\begin{aligned}
L = {} & \frac{1}{2}\left[\dot{X} - \Omega Y + D'\cos(v - M) + D\sin(v - M)\left(\Omega - (v - M)'\right)\right]^2 \\
& + \frac{1}{2}\left[\dot{Y} + \Omega X - D'\sin(v - M) + D\cos(v - M)\left(\Omega - (v - M)'\right)\right]^2 \\
& + \frac{GM_{moon}}{R} - \frac{G}{4R^3}(I_{xx} + I_{yy} + I_{zz}) \\
& + \frac{3G}{4R^5}\left[X^2(I_{yy} + I_{zz} - I_{xx})\right] \\
& + \frac{3G}{4R^5}\left[Y^2(I_{xx} + I_{zz} - I_{yy})\right] \\
& + \frac{GM_{Mars}}{d}\left[1 + \frac{J_2}{2}\left(\frac{R_{Mars}}{d}\right)^2\right] \\
& + \frac{GM_{sun}d^2}{2\rho_{sun}^3}\left(3(\cos S)^2 - 1\right)
\end{aligned}
\tag{62}
$$

23

Generalized Momenta. The generalized momenta are derived as

$$P_X = \frac{\partial L}{\partial \dot{X}} = \dot{X} - \Omega Y + D' \cos(v - M) + D \sin(v - M)\left(\Omega - (v - M)'\right)$$

(63)

$$P_Y = \frac{\partial L}{\partial \dot{Y}} = \dot{Y} + \Omega X - D' \sin(v - M) + D \cos(v - M)\left(\Omega - (v - M)'\right)$$

(64)

When compared to equation (25), it is useful to note that the generalized momenta equations are the inertial velocity components resolved on the moon axes and will be used later to determine initial momenta values.

Generalized Velocities. Now the generalized velocities $(\dot{Q}_i)$ may be eliminated from the Lagrangian. Equations (63) and (64) are rearranged to solve for $\dot{X}$ and $\dot{Y}$

$$\dot{X} = P_X + \Omega Y - D' \cos(v - M) - D \sin(v - M)\left(\Omega - (v - M)'\right)$$

(65)

$$\dot{Y} = P_Y - \Omega X + D' \sin(v - M) - D \cos(v - M)\left(\Omega - (v - M)'\right)$$

(66)

which are then substituted back into the Lagrangian to give

$$L = \frac{1}{2}\left[P_X^2 + P_Y^2\right] + \frac{GM_{moon}}{R} - \frac{G}{4R^3}(I_{xx} + I_{yy} + I_{zz})$$
$$+ \frac{3G}{4R^5}\left[X^2(I_{yy} + I_{zz} - I_{xx})\right] + \frac{3G}{4R^5}\left[Y^2(I_{xx} + I_{zz} - I_{yy})\right]$$
$$+ \frac{GM_{Mars}}{d}\left[1 + \frac{J_2}{2}\left(\frac{R_{Mars}}{d}\right)^2\right] + \frac{GM_{sun}d^2}{2\rho_{sun}^3}(3(\cos S)^2 - 1)$$

(67)

The Lagrangian is now in the correct form to use equation (1).

Hamiltonian. From equation (1) the Hamiltonian can be written as

$$
\begin{aligned}
H = \; & P_X \left(P_X + \Omega Y - D' \cos(v - M) - D \sin(v - M)\left(\Omega - (v - M)'\right)\right) \\
& + P_Y \left(P_Y - \Omega X + D' \sin(v - M) - D \cos(v - M)\left(\Omega - (v - M)'\right)\right) \\
& - \frac{1}{2}\left[P_X^2 + P_Y^2\right] - \frac{GM_{moon}}{R} + \frac{G}{4R^3}(I_{xx} + I_{yy} + I_{zz}) \\
& - \frac{3G}{4R^5}\left[X^2\left(I_{yy} + I_{zz} - I_{xx}\right)\right] - \frac{3G}{4R^5}\left[Y^2\left(I_{xx} + I_{zz} - I_{yy}\right)\right] \\
& - \frac{GM_{Mars}}{d}\left[1 + \frac{J_2}{2}\left(\frac{R_{Mars}}{d}\right)^2\right] - \frac{GM_{sun}d^2}{2\rho_{sun}^3}\left(3(\cos S)^2 - 1\right)
\end{aligned}
\tag{68}
$$

or with some simplification as

$$
\begin{aligned}
H = \; & P_X \left(\Omega Y - D' \cos(v - M) - D \sin(v - M)\left(\Omega - (v - M)'\right)\right) \\
& + P_Y \left(- \Omega X + D' \sin(v - M) - D \cos(v - M)\left(\Omega - (v - M)'\right)\right) \\
& + \frac{1}{2}\left[P_X^2 + P_Y^2\right] - \frac{GM_{moon}}{R} + \frac{G}{4R^3}(I_{xx} + I_{yy} + I_{zz}) \\
& - \frac{3G}{4R^5}\left[X^2\left(I_{yy} + I_{zz} - I_{xx}\right)\right] - \frac{3G}{4R^5}\left[Y^2\left(I_{xx} + I_{zz} - I_{yy}\right)\right] \\
& - \frac{GM_{Mars}}{d}\left[1 + \frac{J_2}{2}\left(\frac{R_{Mars}}{d}\right)^2\right] - \frac{GM_{sun}d^2}{2\rho_{sun}^3}\left(3(\cos S)^2 - 1\right)
\end{aligned}
\tag{69}
$$

25

Hamilton's Equations. The equations of motion can now be written in canonical form which will define the orbital characteristics of the system.

$$\dot{X} = \frac{\partial H}{\partial P_X} = P_X + \Omega Y - D' \cos(v - M) - D \sin(v - M)\left(\Omega - (v - M)'\right) \tag{70}$$

$$\dot{Y} = \frac{\partial H}{\partial P_Y} = P_Y - \Omega X + D' \sin(v - M) - D \cos(v - M)\left(\Omega - (v - M)'\right) \tag{71}$$

$$
\begin{aligned}
\dot{P}_X = -\frac{\partial H}{\partial X} = {} & P_Y\Omega - \frac{GM_{moon}X}{R^3} + \frac{3GX}{4R^5}(3I_{yy} + 3I_{zz} - I_{xx}) \\
& - \frac{15GX}{4R^7}\left[X^2(I_{yy} + I_{zz} - I_{xx}) + Y^2(I_{xx} + I_{zz} - I_{yy})\right] \\
& - \frac{GM_{Mars}(X + D\cos(v\text{-}M))}{d^3}\left[1 + \frac{3J_2R^2_{Mars}}{2d^2}\right] \\
& + \frac{GM_{sun}(X + D\cos(v\text{-}M))}{\rho_{sun}^3}\left(\frac{3A}{(X^2 + Y^2)} - 1\right) \\
& + \frac{GM_{sun}3d^2}{\rho_{sun}^3}\left[\frac{(X(\cos M)^2 - Y\sin M\cos M)}{(X^2 + Y^2)} - \frac{XA}{(X^2 + Y^2)^2}\right]
\end{aligned} \tag{72}
$$

$$
\begin{aligned}
\dot{P}_Y = -\frac{\partial H}{\partial Y} = {} & -P_X\Omega - \frac{GM_{moon}Y}{R^3} + \frac{3GY}{4R^5}(3I_{xx} + 3I_{zz} - I_{yy}) \\
& - \frac{15GY}{4R^7}\left[X^2(I_{yy} + I_{zz} - I_{xx}) + Y^2(I_{xx} + I_{zz} - I_{yy})\right] \\
& - \frac{GM_{Mars}(Y - D\sin(v\text{-}M))}{d^3}\left[1 + \frac{3J_2R^2_{Mars}}{2d^2}\right] \\
& + \frac{GM_{sun}(Y - D\sin(v\text{-}M))}{\rho_{sun}^3}\left(\frac{3A}{(X^2 + Y^2)} - 1\right) \\
& + \frac{GM_{sun}3d^2}{\rho_{sun}^3}\left[\frac{(Y(\sin M)^2 - X\sin M\cos M)}{(X^2 + Y^2)} - \frac{YA}{(X^2 + Y^2)^2}\right]
\end{aligned} \tag{73}
$$

letting A be defined as

$$A = (X\cos M - Y\sin M)^2 \qquad (73.1)$$

X-Axis Symmetry

Jansson found that the equations of motion may be transformed using the following relationships

$$x \Rightarrow x$$
$$y \Rightarrow -y$$
$$t \Rightarrow -t$$

without effecting the equations of motion in the rotating coordinate system of the restricted three body problem. The result is a second orbit which is a reflection of the first about the x axis and traversing in the opposite direction from the first orbit. This effectively doubles the number of data points obtained for a given trajectory and is used to duplicate Jansson's surface of section plots. However, it will not be used after perturbations are added to the system since perturbations destroy the symmetry.

IV. Surface of Section Technique

In this problem there are four initial conditions defined, and if an integral of motion exists, solutions of the system may be represented in a three-dimensional subspace for a given value of the constant integral of motion (9:127). This case is not a restricted three-body problem because the eccentricity of the moon is included. Therefore the surface of section technique is not strictly applicable but is used in an attempt to verify if the periodic orbits found by Jansson are realistic and remain stable.

Poincaré's surface of section technique is an analytical technique which is widely used in numerical exploration. The restricted three-body problem has a four dimensional phase space and one known integral of motion. By considering all orbits with a fixed value of the Hamiltonian the resulting group of orbits must fill a three dimensional subspace of the full four dimensional phase space. If a second integral of motion exists, it would further restrict the motion of the orbits and constrain each orbit to lie on a two dimensional surface imbedded in the three dimensional subspace. If a plane (called the surface of section) is passed through this three dimensional subspace in any arbitrary way, the internal structure of the three dimensional subspace can be examined in two dimensions. When a trajectory on the three dimensional manifold passes through the surface of section plane a point of crossing can be plotted. As more points are plotted, stable periodic orbits will be shown as a series of closed curves. If a second integral of motion does not exist, the trajectories can intertwine randomly in the three dimensional subspace eventually filling it up and the

28

plotted points on the surface of section will be chaotic.(8:128)

This technique is used to examine periodic orbits around the Martian moons where the surface of section is defined by the following condition

$$\vec{R} \cdot \vec{V} = 0 \tag{74}$$

or for the planar case under consideration

$$X\dot{X} + Y\dot{Y} = 0 \tag{75}$$

This condition occurs at the satellite's apoapsis and periapsis points. The points where the satellite is farthest from and closest to the moon. These points are plotted in the two dimensional configuration space.

Other surface of section criteria are possible but this one immediately indicates if the trajectory will collide with the moon. If any one of the surface of section points has a magnitude less than that of the moon, it will obviously collide with the moon before completing the orbit.

Stability of Orbits

For a given Hamiltonian value, stable orbits will be found if the surface of section points form closed contours. A periodic orbit will pass through the centers of the closed curves.

If the closed curves intersect one another (unstable equilibrium point or saddle point), unstable orbits may be located which pass through the intersection points.

V. Solution Method

A FORTRAN computer program was written to integrate the equations of motion using the Haming fourth order integration algorithm to produce satellite trajectories. Initial satellite X and Y coordinates are input along with the Hamiltonian. The output is a data file with the surface of section X and Y coordinates that can be plotted by a two-dimensional plotting program.

Initial Conditions

Initial conditions for the state vector (X, Y, P_X, P_Y) must be determined. The initial values of X, Y, and the Hamiltonian are chosen so that the surface of section conditions (equations 74 and 75) are met. Given this, the initial values of P_X and P_Y may be calculated by first obtaining an expression for $\dot{Y}$.

Substituting equations (63) and (64) into the Hamiltonian (69) and combining all the potential energy terms into the quantity V results in the following

$$H = \frac{1}{2}\left[\dot{X}^2 + \dot{Y}^2 - \Omega^2(X^2 + Y^2) - D'^2 - \left(D\left(\Omega - (v\text{-}M)'\right)\right)^2\right]$$
$$+ \Omega D\left(\Omega - (v\text{-}M)'\right)\left[Y\sin(v\text{-}M) - X\cos(v\text{-}M)\right]$$
$$+ \Omega D\left[X\sin(v\text{-}M) + Y\cos(v\text{-}M)\right] + V \qquad (76)$$

Solving equation (75) for $\dot{X}$ gives

$$\dot{X} = \frac{Y}{X}\dot{Y} \qquad (77)$$

30

Substituting equation (77) into equation (76) and rearranging yields

$$(X^2 + Y^2)\ \dot{Y}^2 = 2X^2\left[H - V\ + \frac{1}{2}\Omega^2(X^2 + Y^2) + \frac{1}{2}(D')^2 + \frac{1}{2}\left(D(\Omega - (v\text{-}M)')\right)^2\right]$$
$$- 2X^2\Omega D(\Omega - (v\text{-}M)'\left[Y\sin(v\text{-}M) - X\cos(v\text{-}M)\right]$$
$$- 2X^2\Omega D\left[X\sin(v\text{-}M) + Y\cos(v\text{-}M)\right]$$

(78)

Solving equation (78) for $\dot{Y}$ results in two values which Jansson found to yield the same trajectory but traveling in opposite directions (prograde and retrograde) for the restricted three-body problem with zero eccentricity.

$\dot{X}$ may be calculated by equation (75) and then the required initial values for P_X and P_Y may be determined from equations (63) and (64).

Trajectory Integration

Haming's Ordinary Differential Equation Integrator is used to numerically integrate the equations of motion. Haming's code is a fourth order predictor-corrector algorithm which is numerically very stable and provides high accuracy. It extrapolates the last four values of the state vector, predicts the next value, evaluates the equations of motion at the predicted value, and then corrects the value using a higher order polynomial (8:120).

Jansson was able to use an integration step size of 200 seconds for most trajectories but, after adding in the eccentricity to the dynamics, an integration step size of 50-100 seconds was required to prevent numerical

31

integration problems. Even with these large integration step sizes, extremely accurate surface of section points were determined using an interpolating polynomial.

Surface of Section Points

At each integration step, the current value of $\vec{R} \cdot \vec{V}$ is compared to the last and if the sign has changed, the surface of section condition stated in equation (74) has been met.

To obtain accurate values for the surface of section points, a Newton Interpolation Polynomial (10:112) is used with the last four values integrated. Since $\vec{R} \cdot \vec{V}$ is a function of X and Y, inverse interpolation (10:119) is used to determine the X and Y coordinates for which $\vec{R} \cdot \vec{V} = 0$.

Remembering that there is trajectory symmetry about the X axis (for Jansson's problem) gives a reflected surface of section point (X, -Y) for every point (X, Y) obtained from the integration. There will be no reflected surface of section points used once eccentricity is added.

Orbit Checks

Checks are made throughout the integration to ensure the trajectory has not escaped the moon's gravitational influence or passed too closely to the mass center of the moon which may create a singularity in the integration. If either of these occur, the integration is halted.

Verification of Dynamics Model and Computer Code

Several checks were made to verify that the equations of motion and

the FORTRAN computer code were correct. One check was to observe the Hamiltonian. The Hamiltonian is a constant integral of motion and should remain invariant (to several decimal places) over the entire trajectory and was checked periodically throughout the integration to insure that it was conserved while eccentricity was kept equal to zero.

Another check was to reduce the computer code dynamics to the simple two-body problem. To do this, the gravitational attraction of Mars and the sun, the system rotation, the moon's eccentricity and mass moments of inertia, and the distance from the moon to the origin of the coordinate system were all set to zero. The satellite was then given circular velocity based on an initial position relative to the moon. As expected, the integrated trajectory was circular, returned to the original starting position, and maintained a constant Hamiltonian. When the moon's mass moments of inertia were included, the orbit was no longer circular but the Hamiltonian did remain constant to eight decimal places.

The next check involved setting the gravitational attraction of the moon and the sun, the J_2 term of the geopotential of Mars, and the initial velocity of the satellite to zero. The satellite position was chosen to lead the moon by a small distance. The integrated trajectory showed the satellite remained relatively stationary in the rotating coordinate system, indicating is was in the expected circular orbit about Mars.

Next, previous research output should be reproducible given the same equations of motion and initial conditions. To duplicate Jansson's work, the gravitational attraction of the sun, the J_2 term of the geopotential of Mars, and the eccentricity of the moon about Mars must all be set to

33

zero. A surface of section plot can then be duplicated from his initial conditions.

As expected, the surface of section plots from Jansson were reproduced for both Phobos and Deimos. Typical surface of section plots for Phobos and Deimos are compared to Jansson's work with the same initial conditions and are shown in Figures 4-7.

Initial Positions

For all integration runs the initial position of the satellite was set at (-X, 0) with values of X matching Jansson's periodic orbits. The initial position chosen results in both the initial velocity and the initial momenta in the X direction being equal to zero.
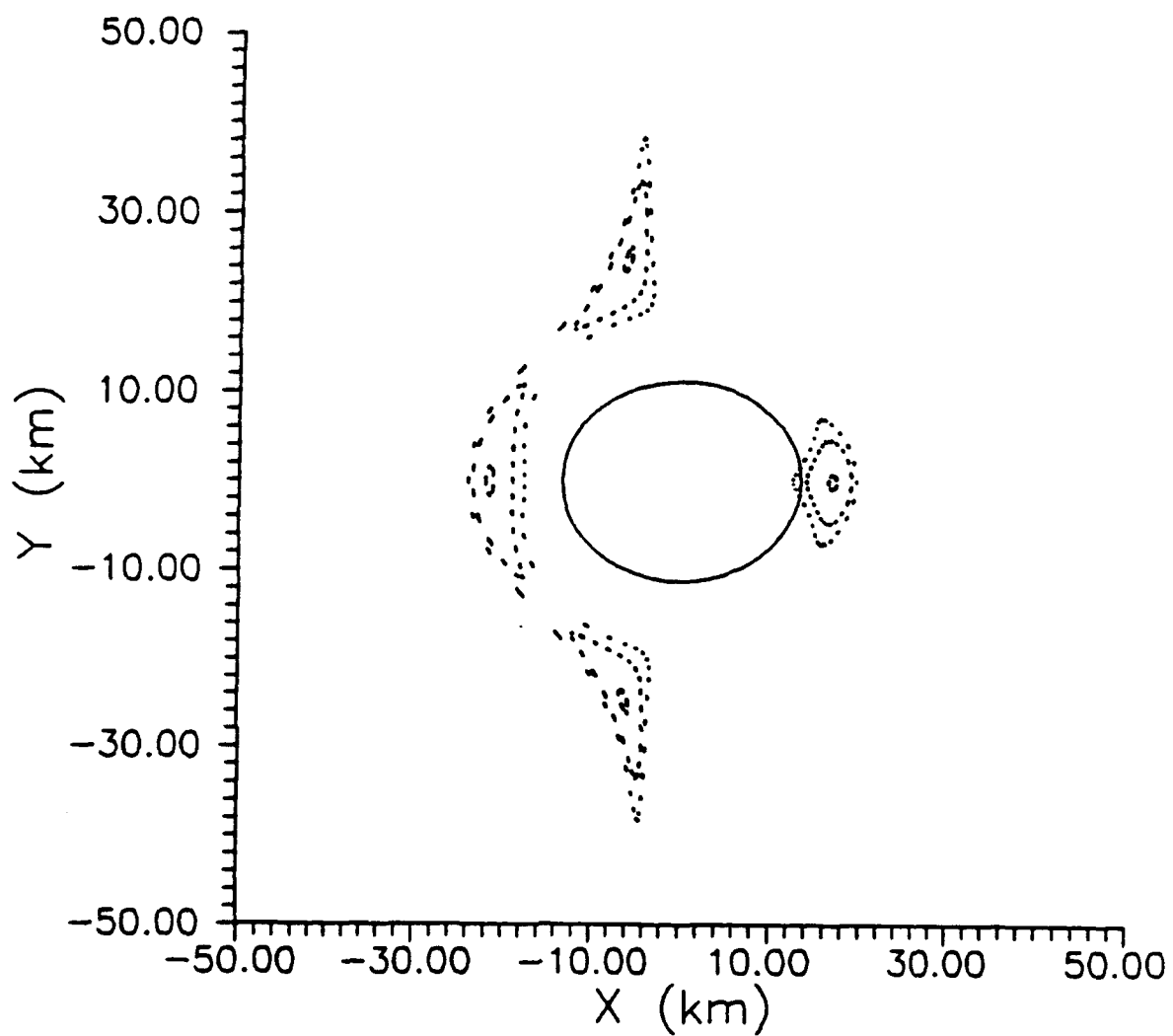
Figure 4. Recreation of Phobos Surface of Section Plot,
H = -6.8528

35
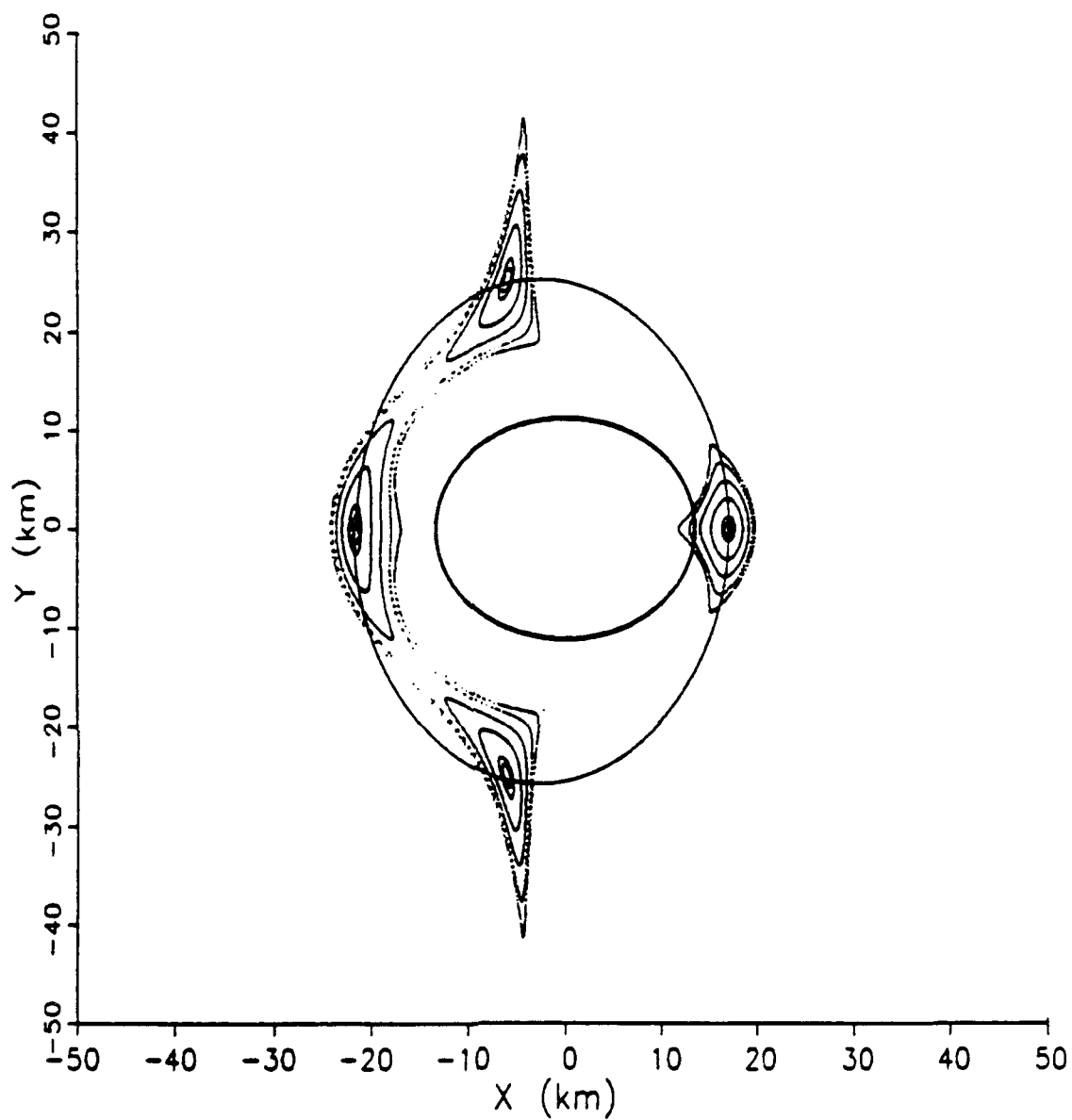
Figure 5. Jansson's Surface of Section Plot for Phobos,
H = -6.8528 (4:32)

3 6
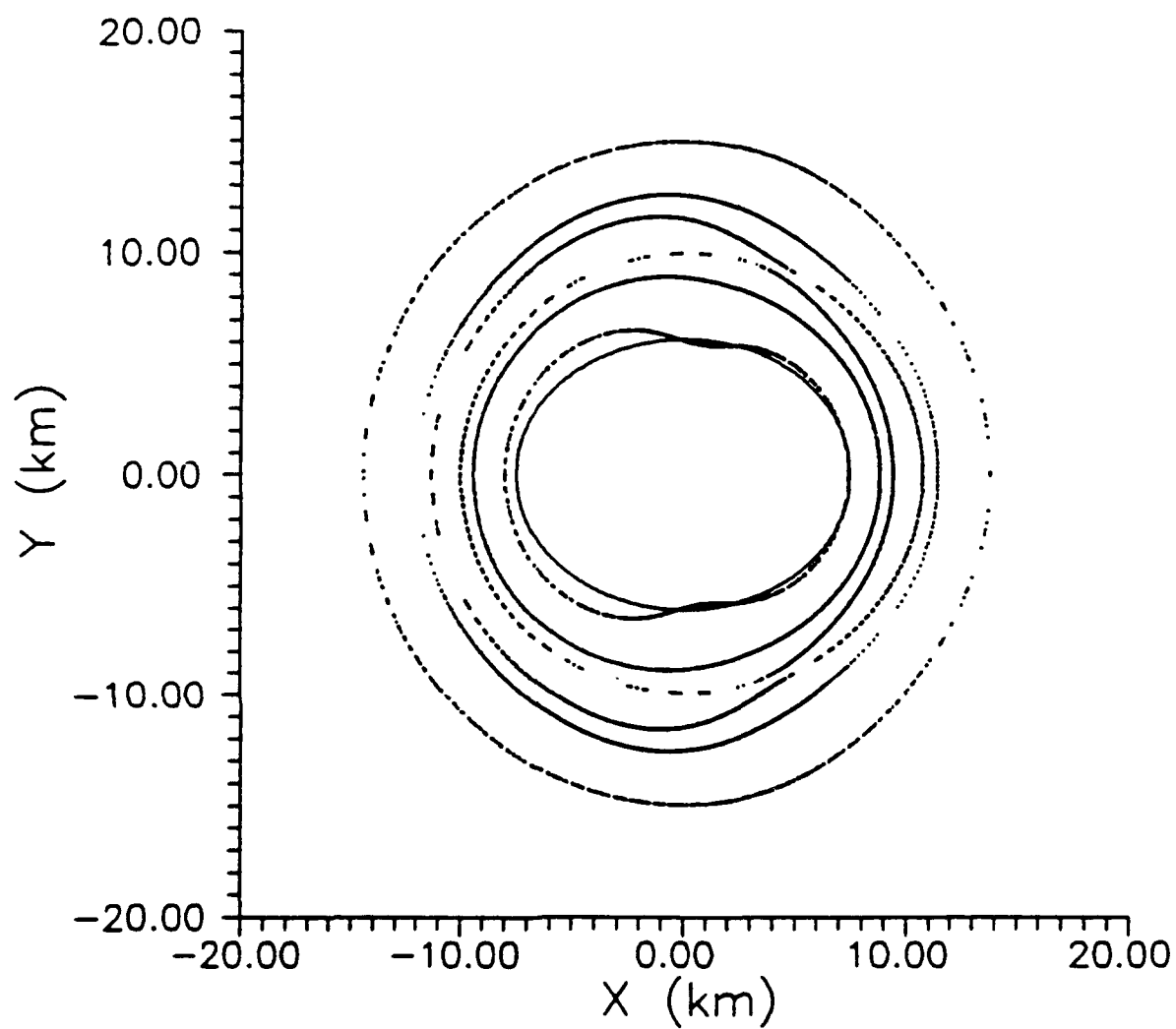
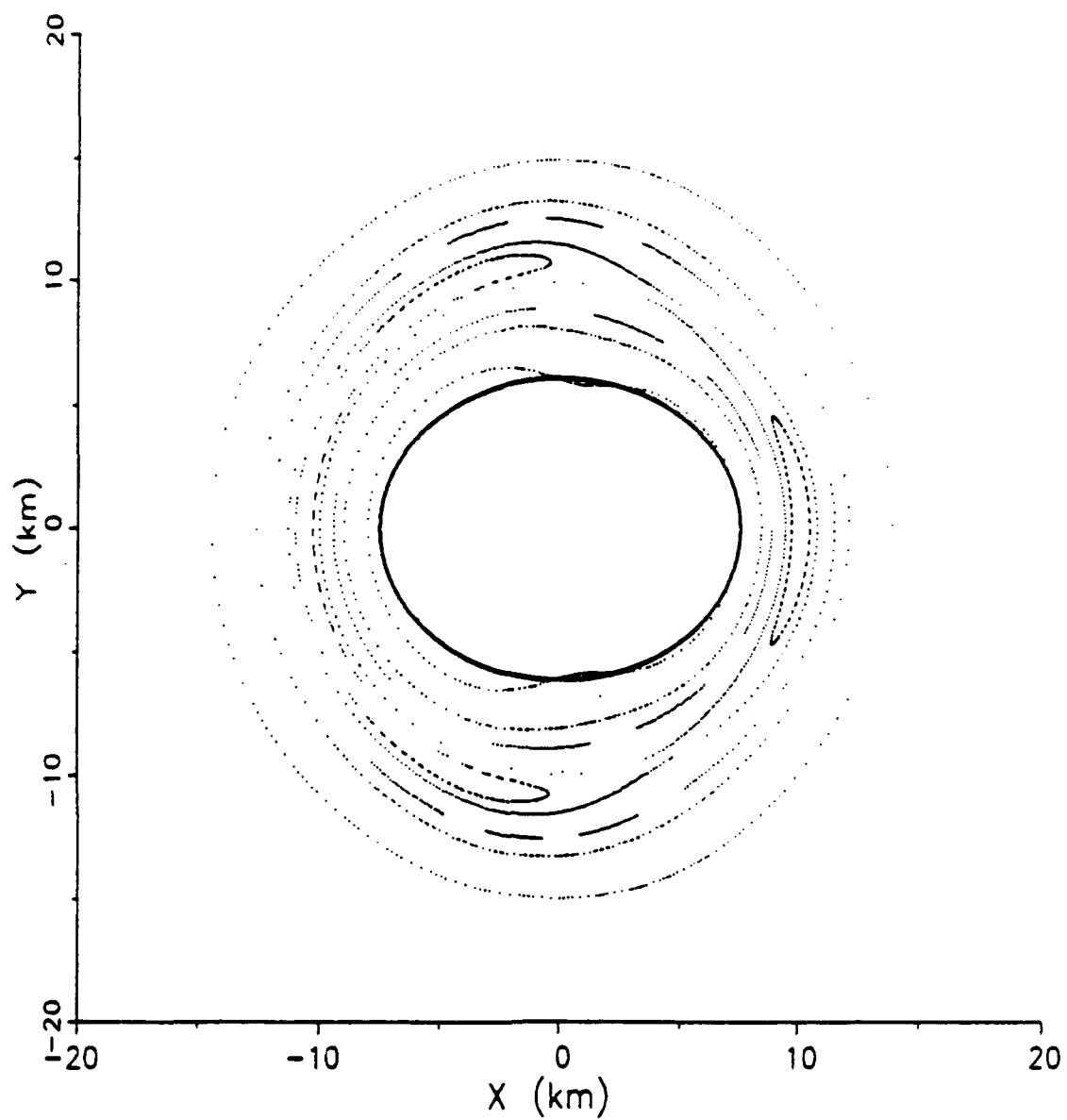Figure 6. Recreation of Deimos Surface of Section Plot,
H = -2.738592

Figure 7. Jansson's Surface of Section Plot for Deimos,
H = -2.738592 (4:52)

VI. Results

With the computer model and dynamics verified the non-circular eccentricity of the moon was introduced to the system. Although the eccentricities of the moons are small, they cannot be ignored for any serious orbital predictions.

As long as the eccentricity was zero, the Hamiltonian could be used to calculate the initial velocity and therefore the initial momenta values as discussed previously. But the Hamiltonian will not remain constant once the eccentricity has been introduced which necessitates a new method of determining the initial momenta values. The first approach tried used the initial velocities as calculated from Jansson's quadratic equation (4:24). This value is identical to equation (78) when the initial conditions are applied. Using this initial velocity proved inappropriate for this problem and resulted in the immediate escape of all trajectories from both Phobos and Deimos. Figure 8 is a plot of a typical trajectory using this initial velocity and clearly shows an eccentric orbit about Mars which is not tracking the revolution rate of the moon about Mars. This indicates that a much more refined initial condition is required.

The momenta can be calculated with a forced value of the orbital period which will match the rates of the orbit to that of the moon with respect to Mars. In the inertial reference frame,

$$\vec{d} = P_X \hat{a}_X + P_Y \hat{a}_Y \tag{79}$$

39

as defined by equations (25) and (63).

Using equation (5) along with the previously stated initial conditions leads directly to

$$v^2 = P_Y^2 \qquad (80)$$

Now using the period of the moon's orbit about Mars (11:33)

$$TP = \frac{2\pi\sqrt{a^3}}{\sqrt{GM_{Mars}}} \qquad (81)$$

solving for the semi-major axis gives

$$a = \sqrt[3]{\frac{(TP)^2 GM_{Mars}}{(2\pi)^2}} \qquad (82)$$

but a can also be written in terms of the specific mechanical energy (11:28)

$$E = -\frac{GM_{Mars}}{2a} \qquad (83)$$

which then gives

$$P_Y = \pm\sqrt{2\left(E + \frac{GM_{Mars}}{d}\right)} \qquad (85)$$

Since the initial position is (-X, 0) and the orbits being investigated are all

40

retrograde, the only possible root for the momenta is the positive one.

The momenta for each periodic orbit found by Jansson (4:33,50) are calculated in the manner described above and are then fixed in the FORTRAN program. Tables 1 and 2 show the results for Phobos and Deimos respectively. The FORTRAN program then uses the fixed values of the momenta to initialize the state vector.

The periodic orbits of the most practical interest for use as parking orbits are the inner orbits, that is the orbits which stay the closest to the moon. The inner orbits did not handle the eccentricity perturbation very well and either collided with the surface of the moon or escaped into an eccentric orbit about Mars. This leads us to the conclusion that our assumption that the orbits are really in orbit about Mars does not hold close in to the moon. Results for each moon will be discussed separately.

Phobos

With only the eccentricity of Phobos added to the system dynamics, the five closest periodic orbits all collided with Phobos ranging from 2.3 days to 45.5 days. The closest orbit (-22,0) made six orbits (2.3 days) before being perturbed into the moon's surface. A trajectory plot for this orbit is shown in Figure 9. If the trajectory is continued, ignoring the surface impact, several more orbits are made before escaping into an eccentric orbit about Mars. Figure 10 shows a typical example of an extended trajectory. Allowing the trajectory to continue after a known collision gives the surface of section plots more data points which may begin to show some useful pattern.

Table 1

Momenta Calculations for Phobos

Initial Condition	P_Y
(-22,0)	2.174818341961
(-68,0)	2.185520332825
(-93,0)	2.191359656599
(-112,0)	2.195808491525
(-129,0)	2.199797095646
(-143,0)	2.203087580257
(-156,0)	2.206147703997
(-169,0)	2.209212347677
(-179,0)	2.2¹1572853458
(-332,0)	2.248029772709
(-708,0)	2.340508386779

Table 2

Momenta Calculations for Deimos

Initial Condition	Py
(-10,0)	1.352473639530
(-13,0)	1.352646614364
(-18,0)	1.352934955024
(-23,0)	1.353223357308
(-31,0)	1.353684929236
(-41,0)	1.354262116378
(-48,0)	1.354666294454
(-56,0)	1.355128360725
(-75,0)	1.356226403753
(-109,0)	1.358193561438
(-135,0)	1.359699802981
(-156,0)	1.359699802981
(-233,0)	1.365392424480
(-340,0)	1.371635636656
(-418,0)	1.376205272893

All five inner periodic orbits followed this same typical pattern and collided with Phobos. A typical surface of section plot is shown in Figure 11 for the (-22,0) orbit and, ignoring the surface impact, shows a non-periodic orbit which escapes into a retrograde orbit about Mars.

Similarly, the six outermost orbits remained in orbit about Phobos much longer than the closer orbits but never repeated the same trajectory and eventually collided with the moon ranging from 9 days to 144 days. Again the surface collision was ignored in order to see if any pattern in the surface of section plot began to emerge. A typical trajectory is shown in Figure 12 for the (-143,0) orbit with uneven axes for visual clarity. Table 3 summarizes the results for each orbit.

The surface of section plots for these orbits all showed the same pattern of non-periodic orbits which, ignoring the surface collision, escape into an eccentric orbit about Mars. Figures 13 and 14 show a surface of section plot for the (-143,0) orbit which clearly indicate the surface impact (on the 48th day) and eventual escape into an eccentric, prograde orbit about Mars. The same pattern is seen in Figures 15 and 16 for the (-156,0) orbit as well as for the remaining outermost orbits.

The most promising case was the (-332,0) orbit which remained around Phobos the longest time (144 days) before its trajectory collided with the surface. Figures 17 and 18 clearly show the collision and subsequent escape of the spacecraft to a prograde orbit about Mars.

With the exception of the (-708,0) orbit, the remaining five outermost periodic orbits remained around Phobos well over 45 days before colliding with the surface. The (-708,0) orbit is the furthest periodic orbit

44

Table 3

Summary of Trajectory Runs for Phobos

Initial Condition	Trajectory
(-22,0)	collision at 2.3 days
(-68,0)	collision at 10.7 days
(-93,0)	collision at 26 days
(-112,0)	collision at 28.6 days
(-129,0)	collision at 45.5 days
(-143,0)	collision at 48 days
(-156,0)	collision at 50.3 days
(-169,0)	collision at 69 days
(-179,0)	collision at 71.3 days
(-332,0)	collision at 144 days
(-708,0)	collision at 9 days

from Phobos found by Jansson and it collided with the surface in only 9 days.

With only the eccentricity of Phobos added to the system dynamics, all the periodic orbits found by Jansson became unstable and collided with the moon. Therefore, no other perturbations were added to the system for study.

Deimos

Table 4 is a summary of the results for the orbits investigated around Deimos with only the eccentricity added to the system dynamics. Again, the inner orbits are of most interest.

With only the eccentricity of Deimos added to the system dynamics, the first seven inner periodic orbits found by Jansson either collided with the surface of Deimos or escaped into an eccentric orbit about Mars. Figures 19 to 25 graphically show the collisions and escapes for these seven orbits which ranged from 2.5 hours to 9.9 days. As expected for the inner orbits, as the orbits moved away from Deimos they increased their orbital periods and improved their chances of remaining in orbit longer. Figure 25 for the orbit at (-48,0) clearly shows six orbits, with a closest approach of about 25 km, before escaping into a retrograde orbit about Mars. The best surface of section plot for the inner orbits is shown in Figure 26 and displays a random scattering of crossings for the (-48,0) orbit.

The eight outermost periodic orbits found by Jansson all behaved much better and stayed around Deimos for the entire integration period of 115 days without colliding with the surface or escaping. In order to see if

Table 4

Summary of Trajectories for Deimos

Initial Condition	Trajectory
(-10,0)	Collision at 2.5 hours
(-13,0)	Escaped at 23.3 hours
(-18,0)	Escaped at 2.1 days
(-23,0)	Escaped at 2.3 days
(-31,0)	Collision at 15 hours
(-41,0)	Collision at 2.3 days
(-48,0)	Escaped at 9.9 days
(-56,0)	Remained for 578 days
(-75,0)	Remained for 578 days
(-109,0)	Remained for 578 days
(-135,0)	Remained for 578 days
(-156,0)	Remained for 578 days
(-233,0)	Remained for 578 days
(-340,0)	Remained for 578 days
(-418,0)	Remained for 578 days

any pattern developed for these outer orbits, the integration period was increased to 578 days. This increased the integration time to over 60 minutes for each run. A typical trajectory plot for the seven outermost orbits is shown in Figure 27 and shows an oscillating eccentric orbit remaining around Deimos. Based on the appearance of the trajectory and the length of the integration period without a collision or escape, these eight outermost orbits are considered stable.

Figure 28 shows the surface of section plot for the (-56,0) orbit and has no closed circles or ellipses which would indicate that there are no periodic orbits. However, since this is a time varying Hamiltonian system the surface of section technique does not strictly apply; if the added perturbation is small enough, one could expect to see the surface of section points collected within some region or boundary. This is clearly seen in Figure 28.

Figures 29 thru 37 show more examples of the surface of section plots for these seven outermost orbits of Deimos. Although not as random in pattern as in Figure 28, they do appear as if they will fill in the same bounded area but at a much slower pace. Several close-up views are presented to get a better look at the structure. These close-up views clearly show there are no closed circles or ellipses and that they appear as if they will loop back and continue to fill in the same bounded area as in Figure 28.

When the J_2 term of Mars' geopotential was added to the the system dynamics the (-56,0) orbit also went unstable and collided with the moon after 130 days. The last seven orbits continued to remain stable.

VII. Conclusions

All integration runs were made with just the eccentricity of the moons added to the system dynamics. Since all of the periodic orbits previously found around Phobos became unstable, no other perturbations needed to be introduced to the system to prove the orbits were unrealistic. In a similar manner, the seven innermost periodic orbits of Deimos which are of more practical use also became unstable with just the eccentricity of Deimos added to the system dynamics.

Phobos

It is quite clear that for Phobos all the periodic orbits found by Jansson were based on the assumption that the orbit of Phobos was circular. However, the true eccentricity of .015 proved to be too large of a perturbation for the assumption to hold and all the orbits became unstable and collided with the surface of Phobos. Even though the orbits are not periodic in nature, any spacecraft attempting to rendezvous with another planet will have the capability to make station keeping maneuvers. With the range of orbital times from 2.3 days to 144 days, there are plenty of opportunities for these type of corrections. It is unfortunate that the closest two orbits collide with Phobos in less than 11 days making them unsafe as choices for a parking orbit even with station keeping. The next closest orbit is located at (-93,0) and gives a reasonable safety margin to make a station-keeping maneuver before colliding with the surface in 26 days. With the exception of the (-708,0) orbit, the safety margins increased with

49

increasing distance from Phobos, allowing more flexibility but at the same time reducing its desirability as a parking orbit.

The (-708,0) orbit is the furthest away from Phobos and, as seen in Table 3, did not follow the expected trend of increasing orbital time before a collision occurred. This is may be due to the satellite's attempt to enter a true orbit around Phobos instead of an eccentric orbit around Mars, that stays close to Phobos. This attempt is doomed by the fixed initial momenta value based on Phobos' revolution rate around Mars.

Deimos

Because of the much smaller eccentricity of Deimos than Phobos and the much larger distance from Mars, the orbits around Deimos were expected to behave better than those of Phobos. The seven innermost orbits still did not handle the eccentricity perturbation very well and either collided or escaped rather rapidly. The eighth orbit (-56,0) went unstable with the addition of the geopotential term of Mars while the seven outer-most orbits did settle down into an acceptable stable condition.

Of the seven innermost orbits, four escaped from Deimos and there-fore could be used safely without fear of imminent collision with the sur-face. Of course station keeping maneuvers could easily be made to keep the spacecraft around indefinitely. The three collision orbits ranged in orbital time from 2.5 hours to 9.9 days and may not be safe choices for parking orbits even with station keeping.

Although the seven outermost orbits of Deimos did appear to be stable they are not considered very useful for a Mars mission due to their

50

much larger distance from the Martian surface and larger distances from Deimos itself which increases its orbital period and decreases its usefulness as a way-station. Additionally, the much larger distance from Deimos to Mars realistically means there will be a negligible effect from the J_2 term of the geopotential, and the perturbing force of the sun can realistically be considered negligible. For these reasons, and the fact that Phobos is considered a more useful choice for a way-station, the perturbing force of the sun was not added to the dynamics to fully test the seven outermost orbits of Deimos.

These seven outermost orbits did remain around Deimos for the entire integration period of 578 days, oscillating along the Y axis of Deimos, as shown in the figures described earlier. The surface of section plots indicate a boundary constraining the points and was expected for small perturbations. Any one of these seven orbits could be used as a parking orbit for Deimos without the need for any station keeping maneuvers. Realistically, only the orbits under 100 km would most likely be considered as serious candidates for parking orbits, and only if Deimos is seriously considered as a way-station over Phobos.

Appendix A Problem Parameters (4:67)

Moons:	Phobos	Deimos
Axis Lengths (km)	x = 13.4	x = 7.5
	y = 11.2	y = 6.1
	z = 9.2	z = 5.2

Moments of Inertia ($kg*km^2$)

$$Ixx = 42.016 * M_{moon} \qquad Ixx = 12.850 * M_{moon}$$
$$Iyy = 52.840 * M_{moon} \qquad Iyy = 16.658 * M_{moon}$$
$$Izz = 61.000 * M_{moon} \qquad Izz = 18.692 * M_{moon}$$

Average Semi-Major Axis Radius (km)

$$a = 9,378 \qquad\qquad a = 23,459$$

Rotation Rate (rad/sec)

$$\Omega = 0.000228 \qquad\qquad \Omega = 0.0000576$$

Gravitational Parameter (km^3/sec^2)

$$GM_{moon} = 0.00066 \qquad\qquad GM_{moon} = 0.000088$$

Orbital Eccentricity (12:6.28)

$$e = 0.015 \qquad\qquad e = 0.00052$$

Mars:

Gravitational Parameter (km^3/sec^2)	$GM_{Mars} = 42828.32$
Equatorial Radius (km) (12:6.3)	$R_{Mars} = 3397.2$
Geopotential Coefficient (12:6.7)	$J_2 = .0019557$

52

Appendix B <u>Phobos Figures</u>

Figure 8. Example Trajectory with Mismatched Orbital Periods
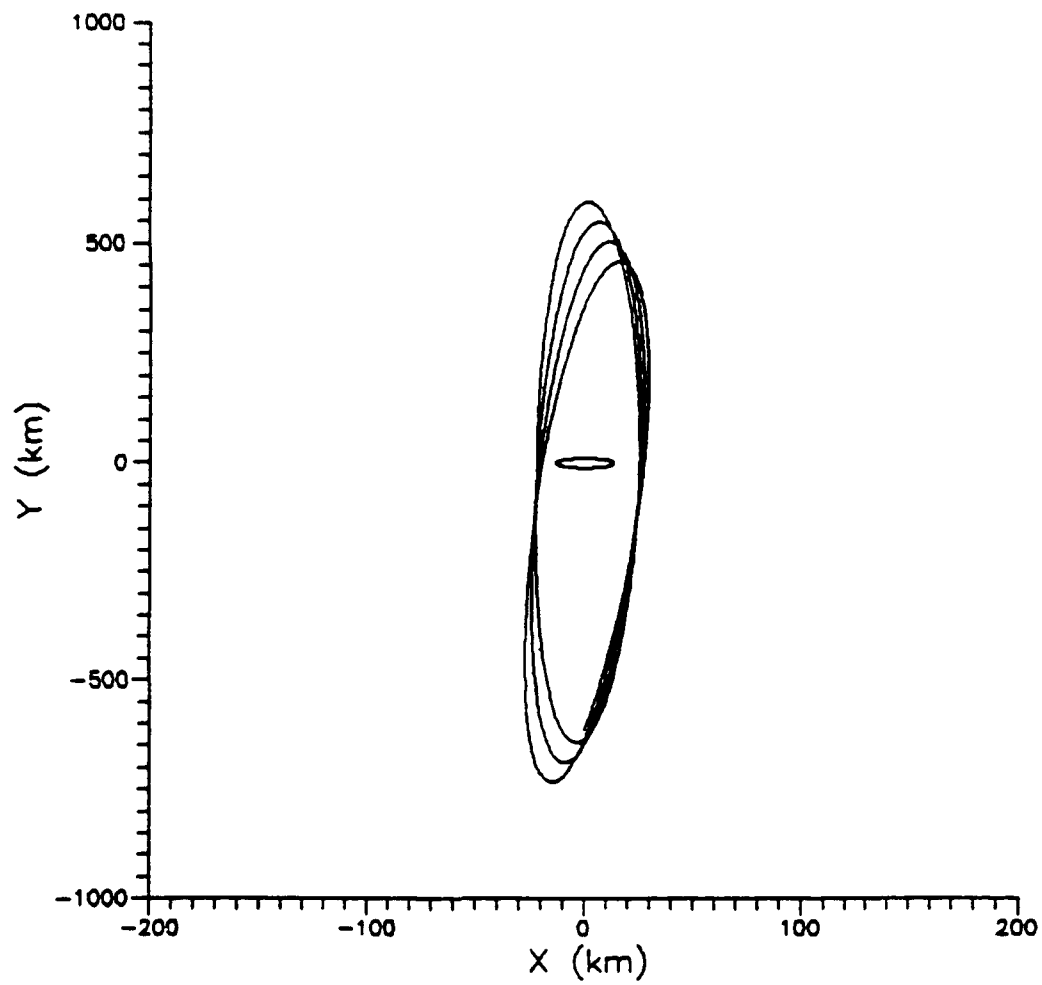
Figure 9. Collision Trajectory for Orbit (-22,0)

5 5
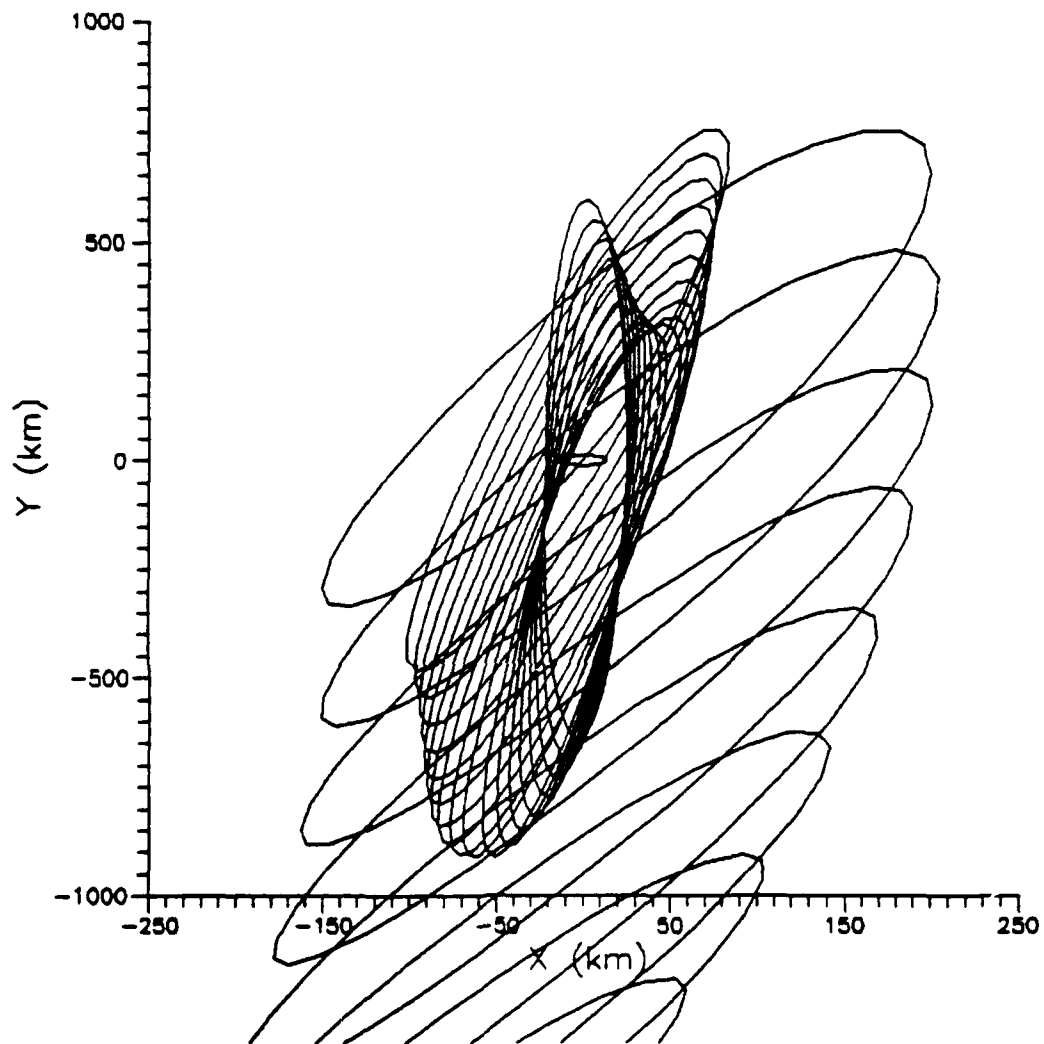
Figure 10. Extended Trajectory for Orbit (-22,0)

56
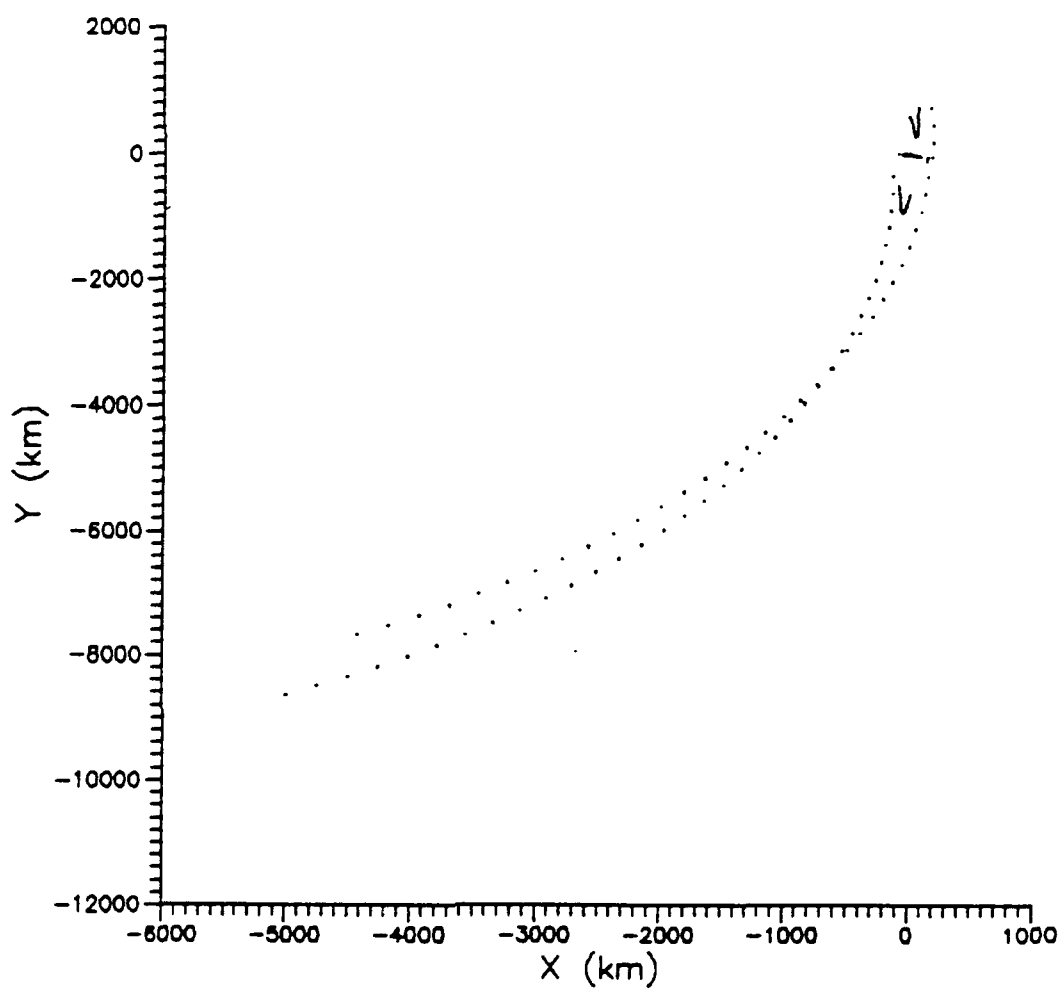
Figure 11. Surface of Section Plot for Orbit (-22,0)

57
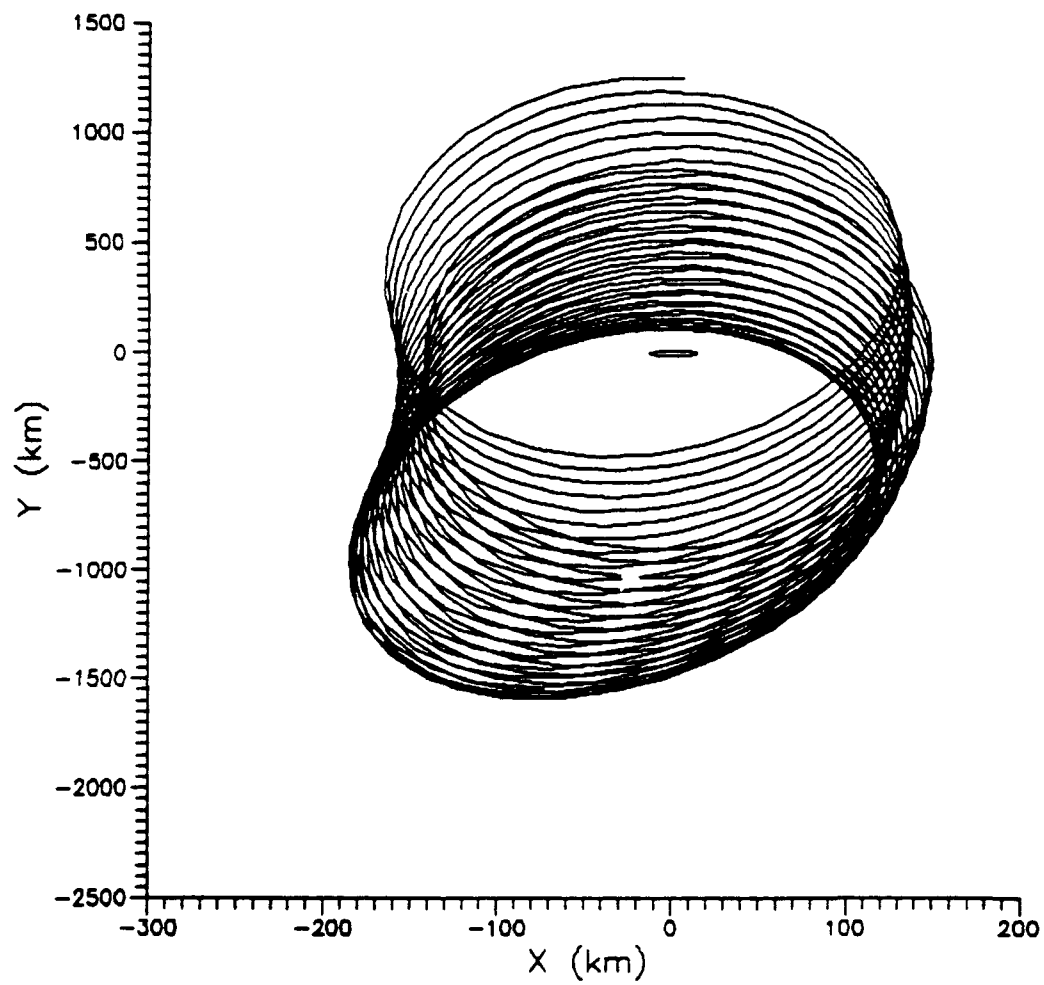
Figure 12. Collision Trajectory for Orbit (-143,0)
(Note uneven scale for visual clarity)

5 8
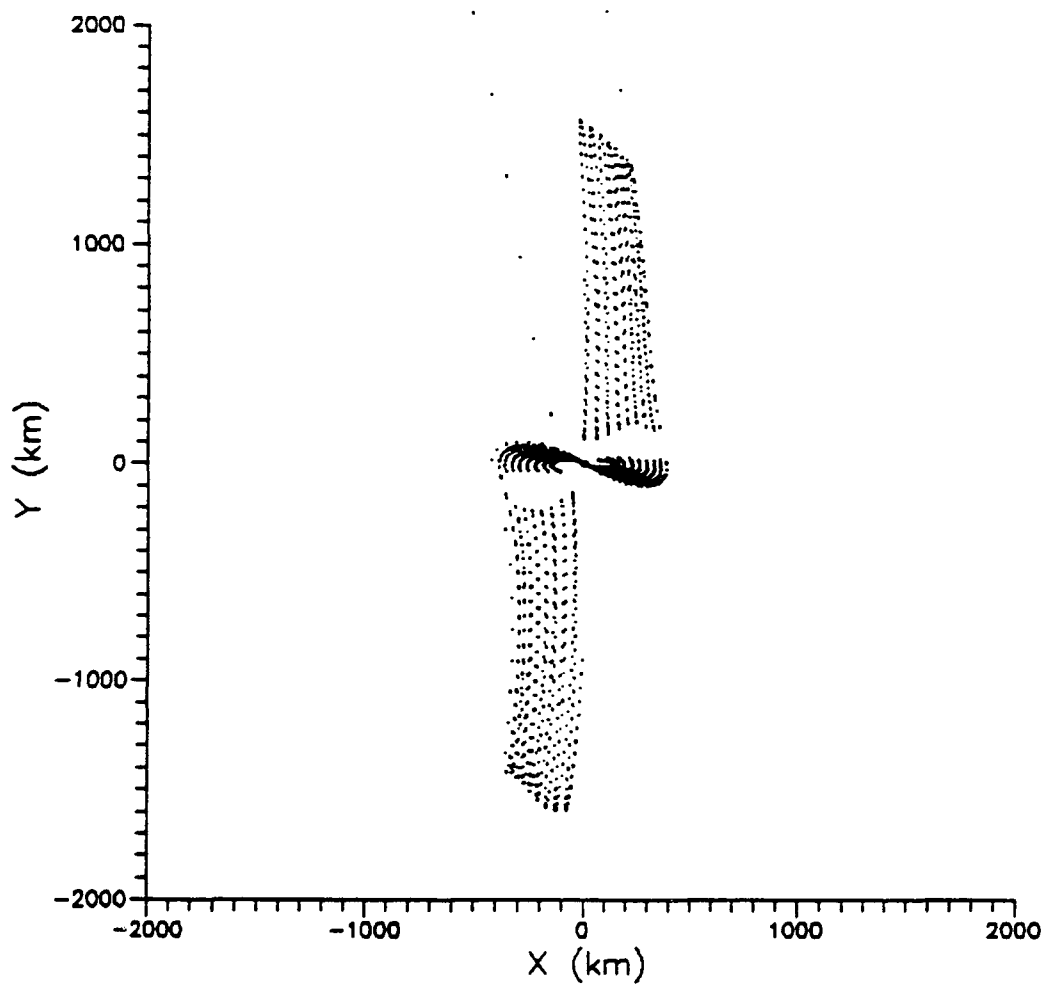
Figure 13. Surface of Section Plot for Orbit (-143,0)
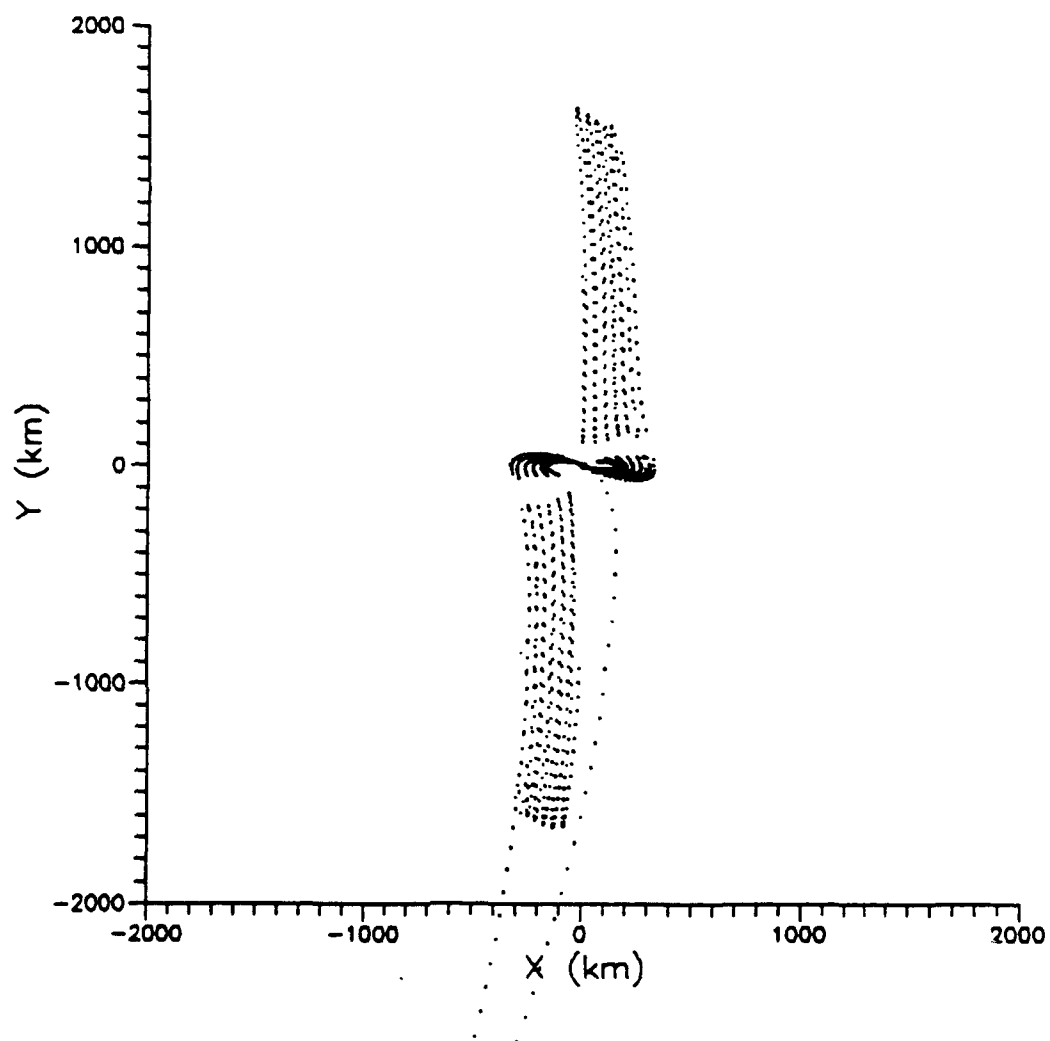
59
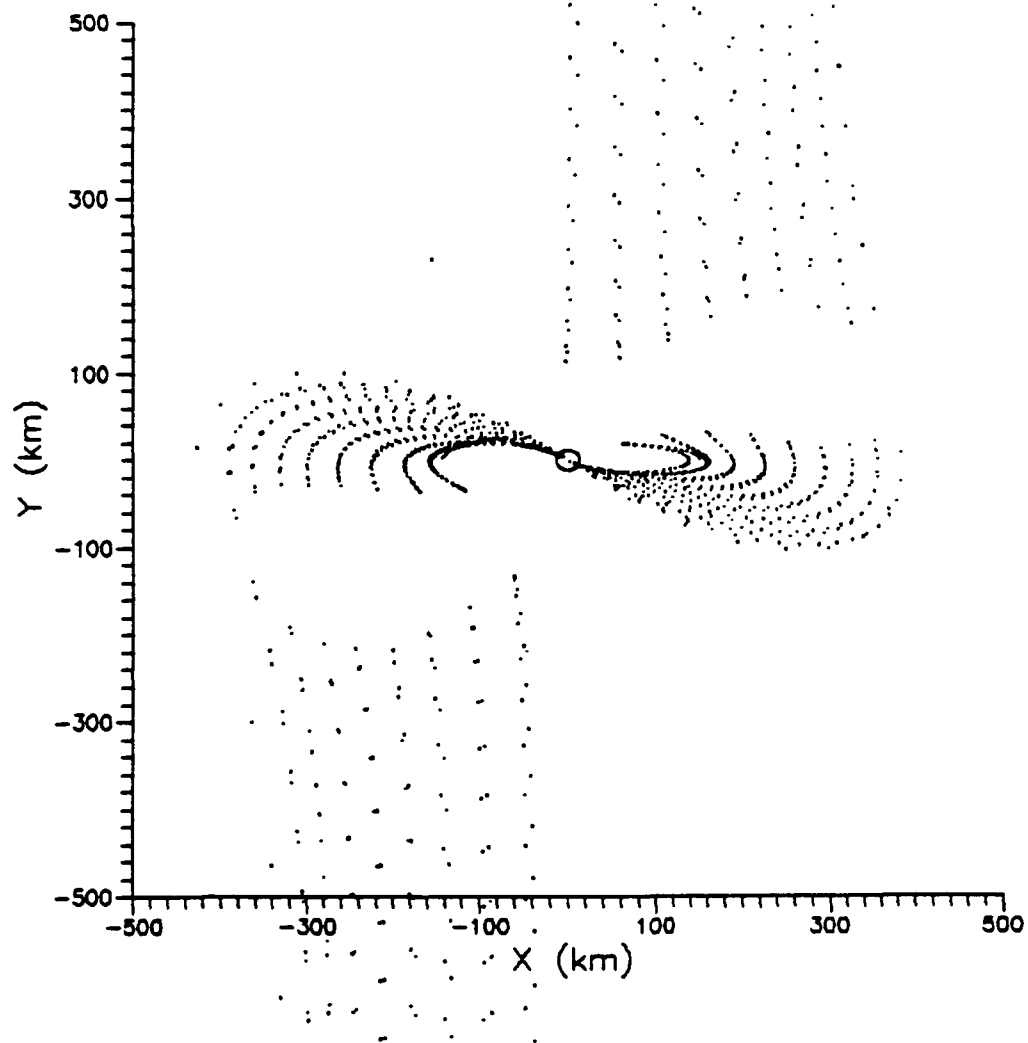
Figure 14. Surface of Section Plot for Orbit (-143,0)

60

Figure 15. Surface of Section Plot for Orbit (-156,0)

6 1
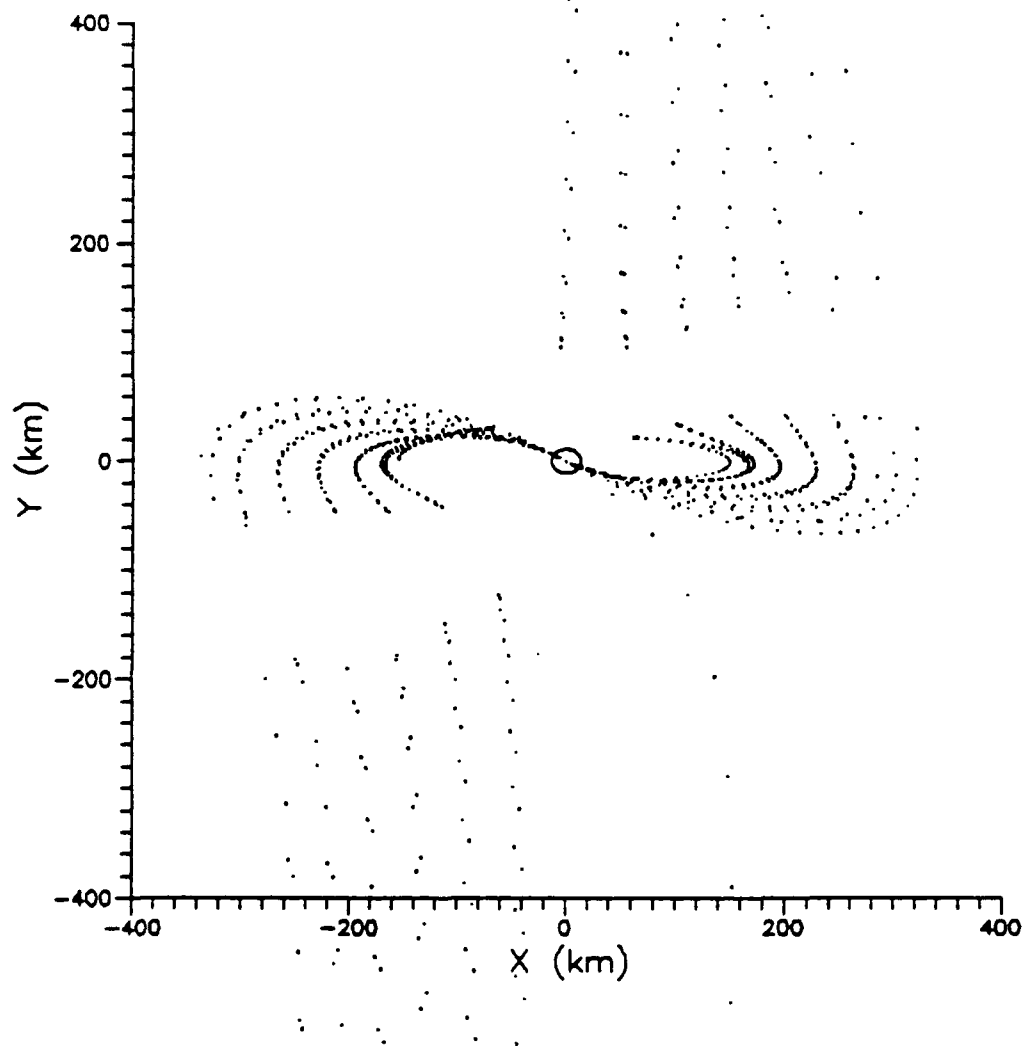
Figure 16. Surface of Section Plot for Orbit (-156,0)
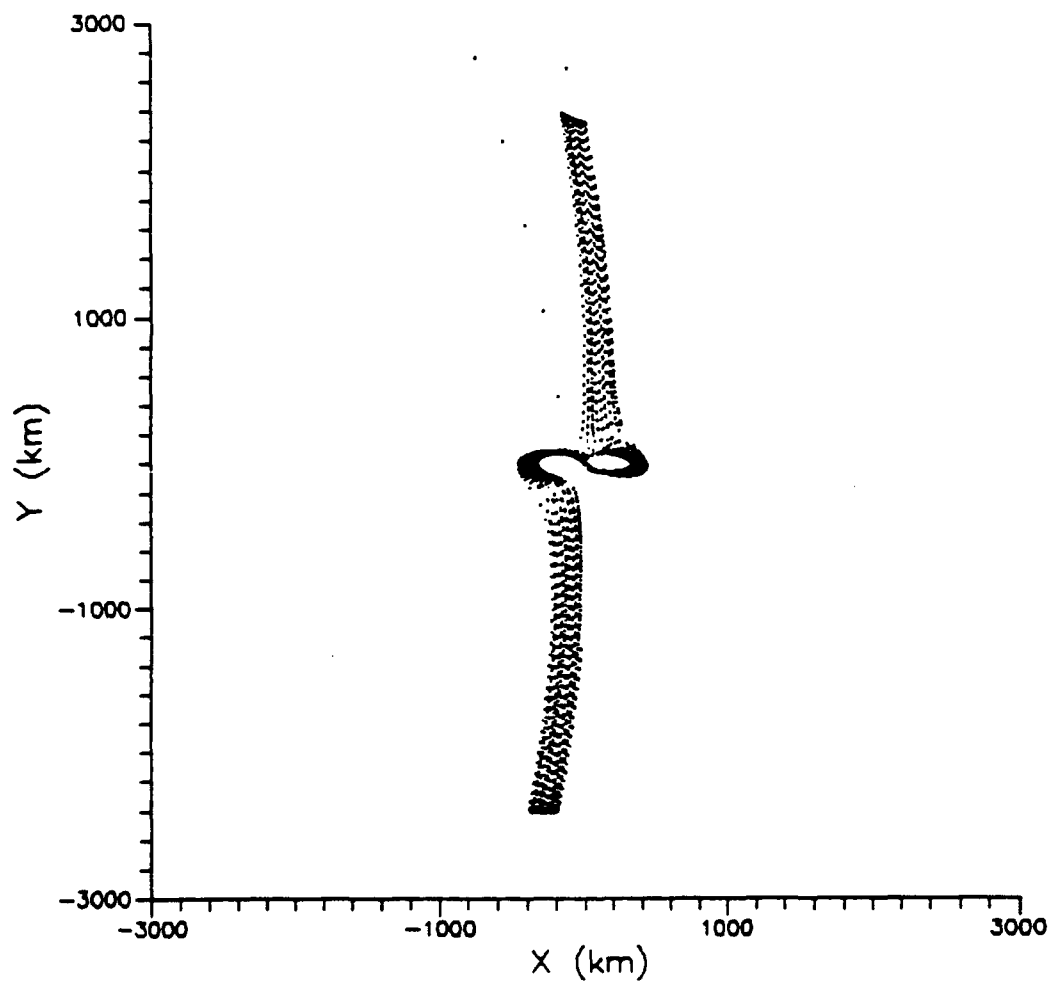
Figure 17. Surface of Section Plot for Orbit (-332,0)
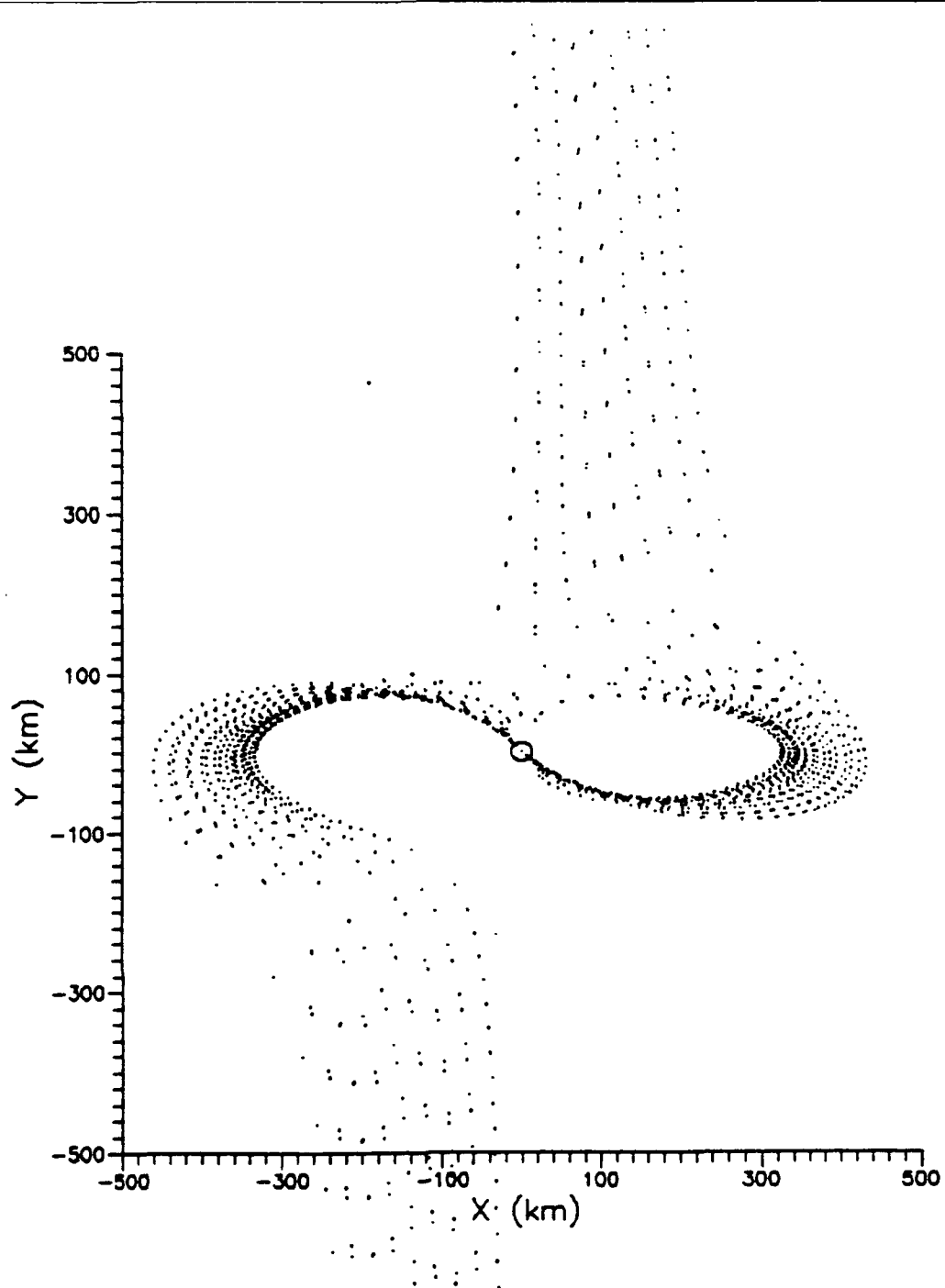
Figure 18. Surface of Section Plot for Orbit (-332,0)
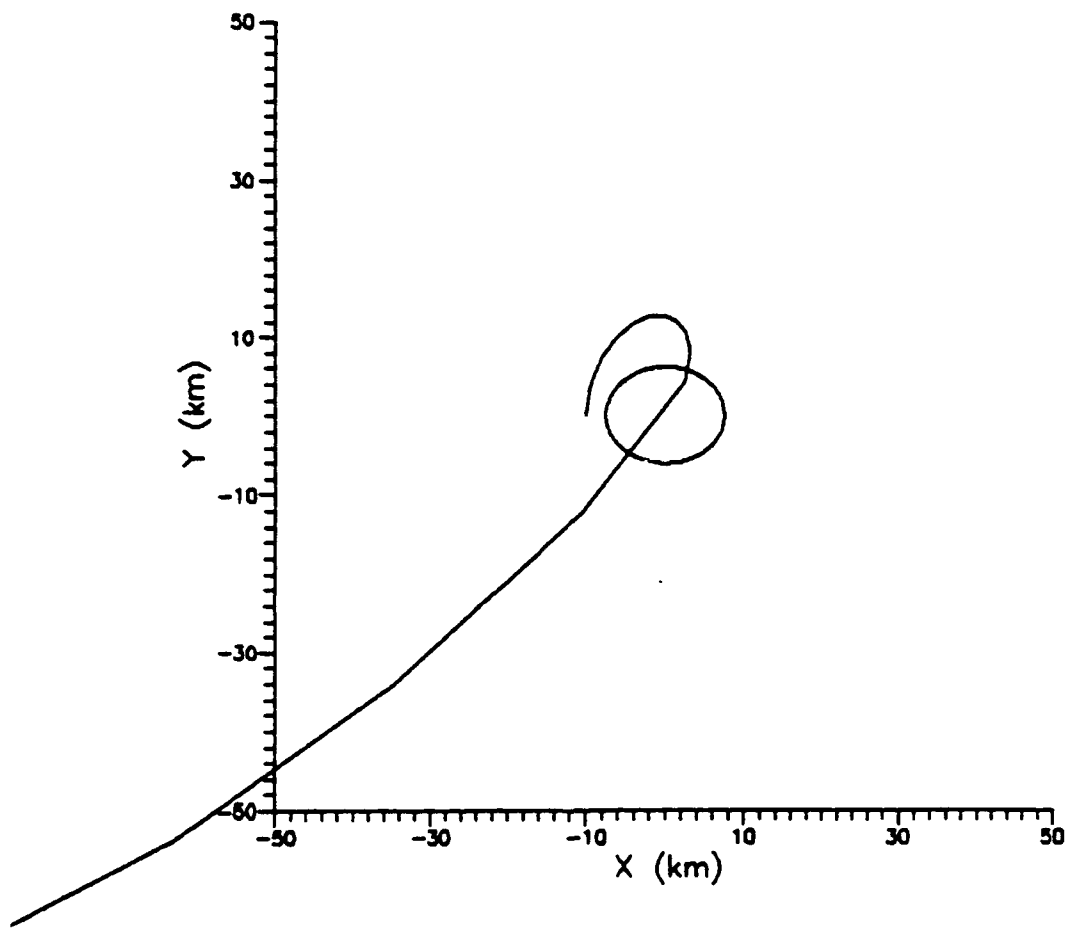
6 4

Appendix C Deimos Figures
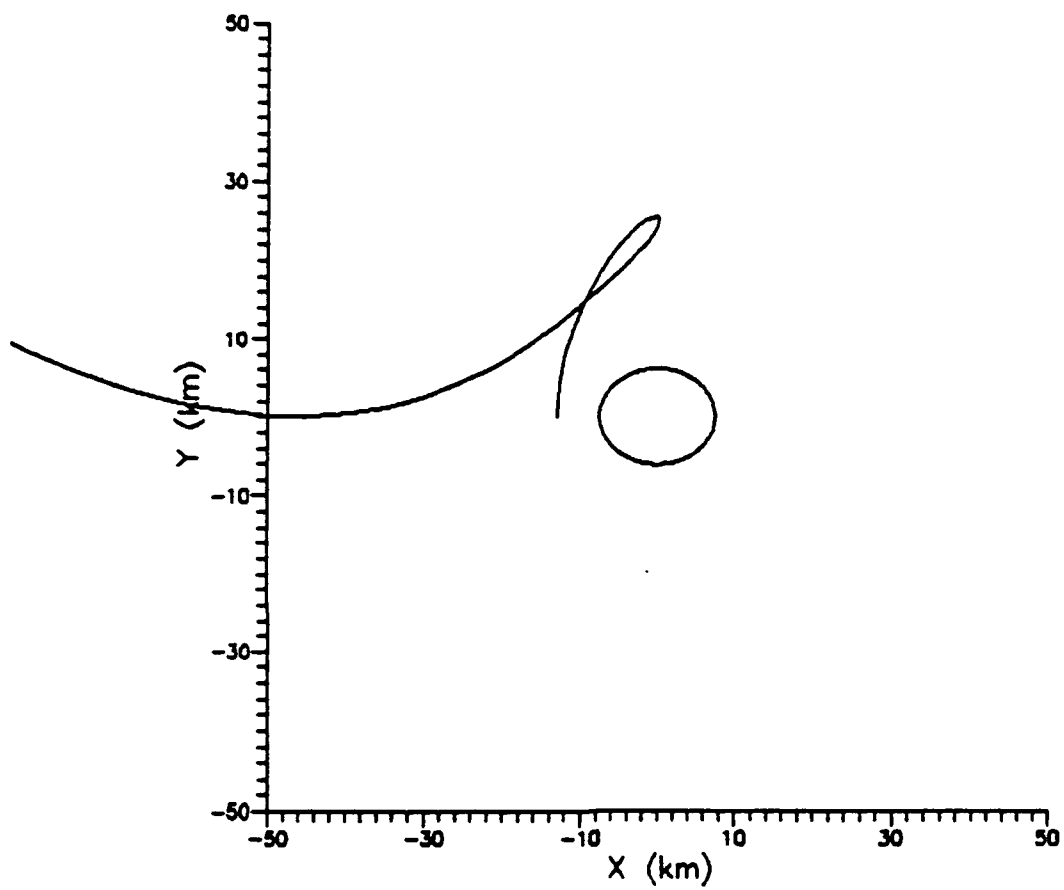
Figure 19. Collision Trajectory for Orbit (-10,0)
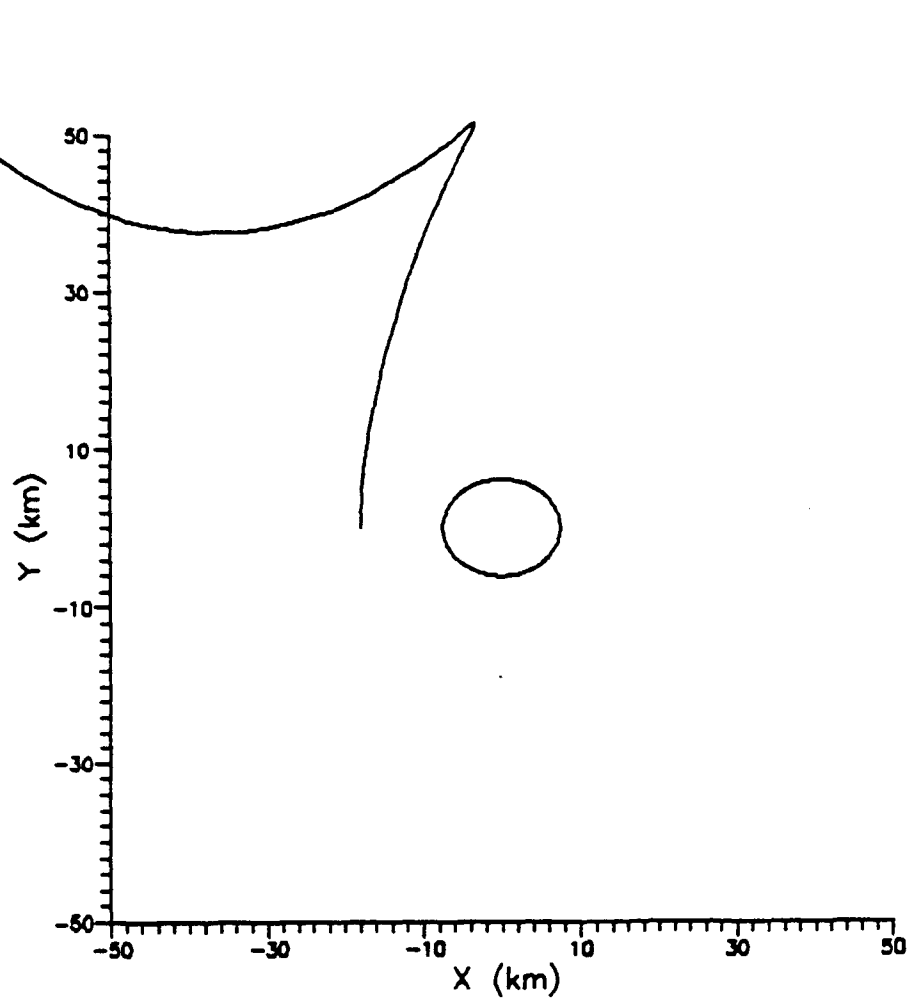
Figure 20. Escape Trajectory for Orbit (-13,0)

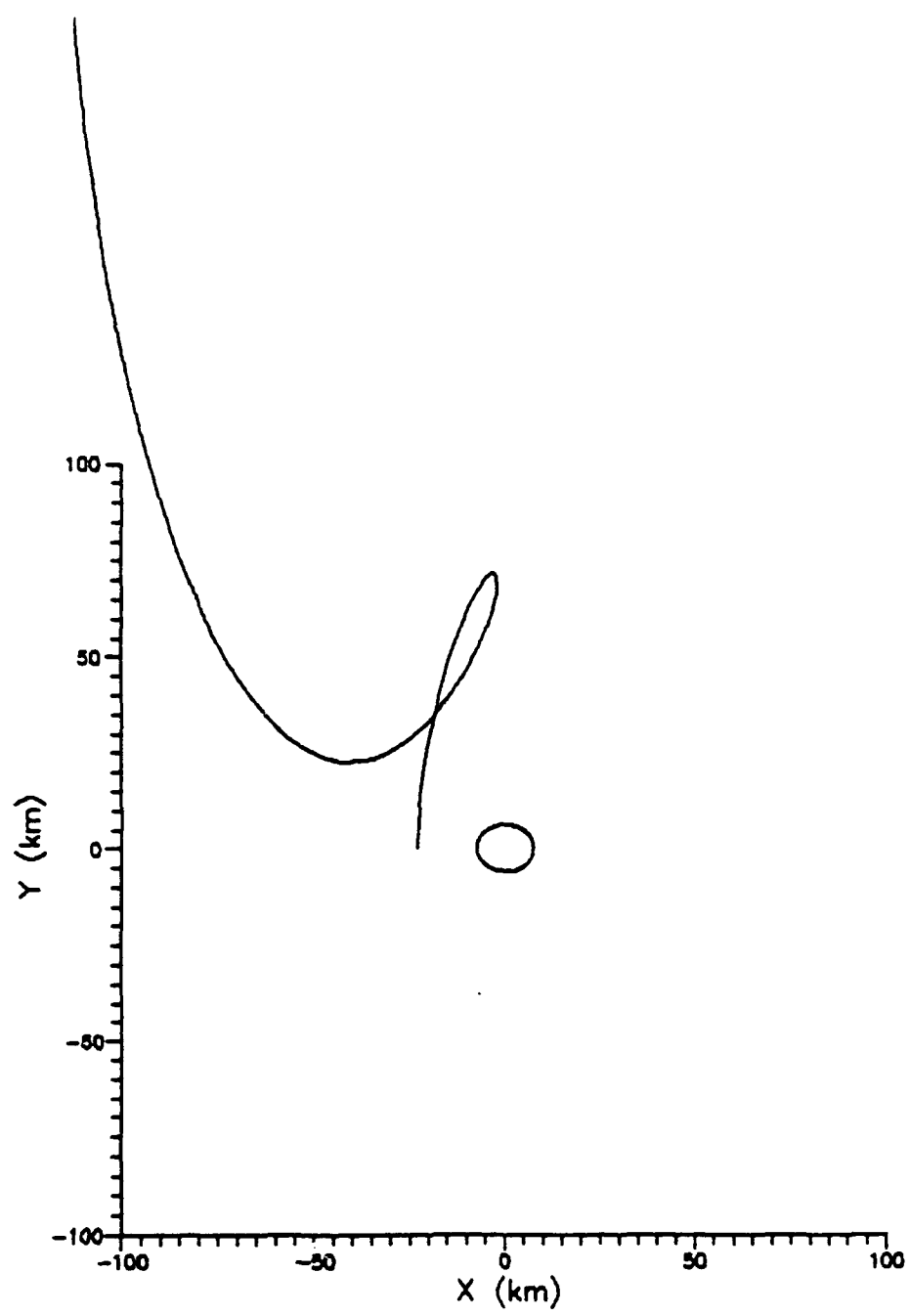Figure 21. Escape Trajectory for Orbit (-18,0)

Figure 22. Escape Trajectory for Orbit (-23,0)

69
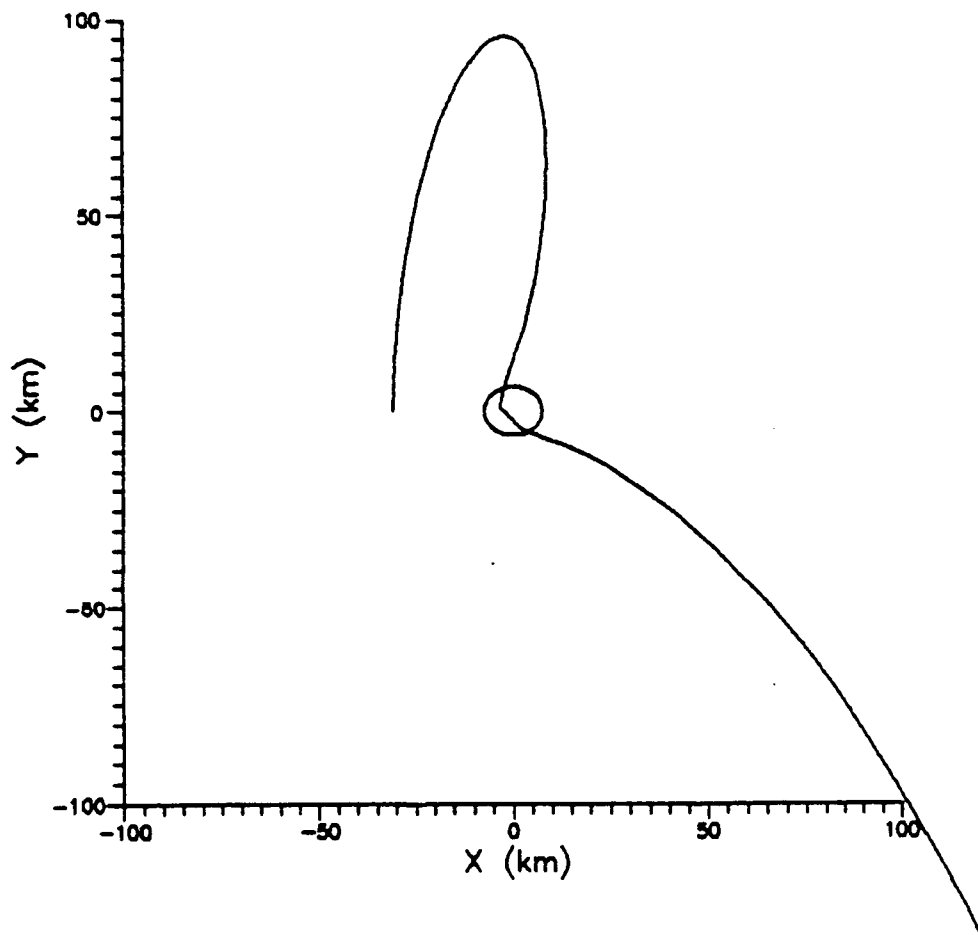
Figure 23. Collision Trajectory for Orbit (-31,0)

70
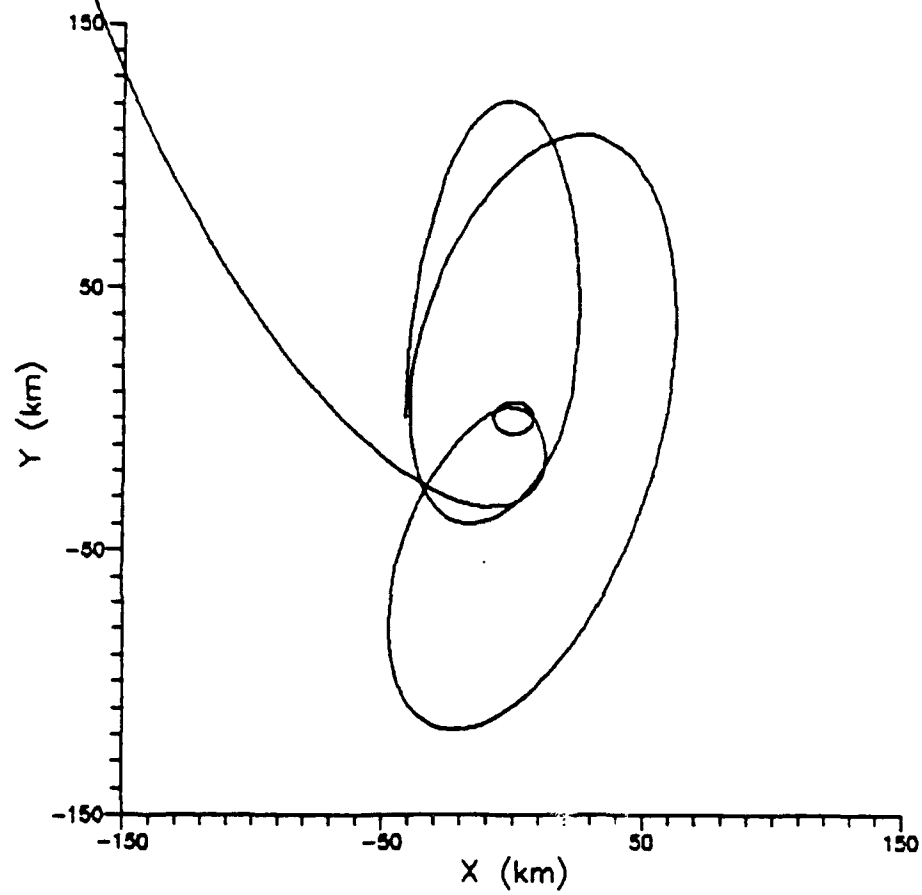
Figure 24. Collision Trajectory for Orbit (-41,0)
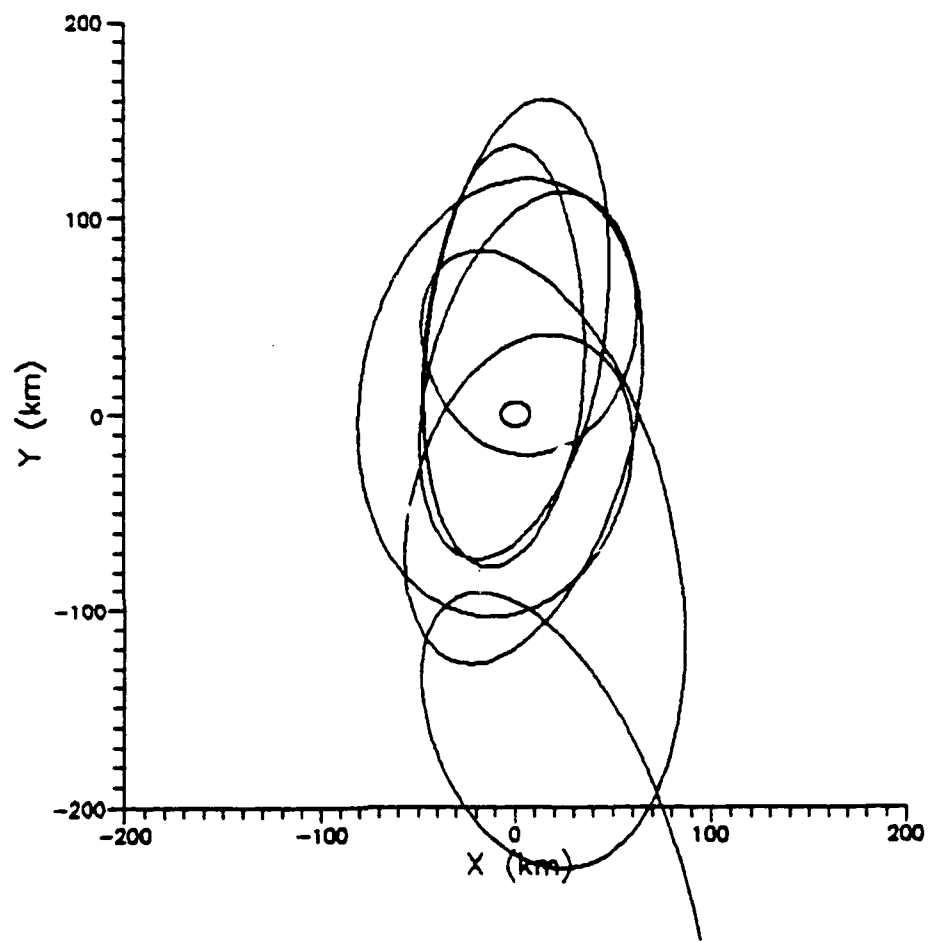
Figure 25. Escape Trajectory for Orbit (-48,0)
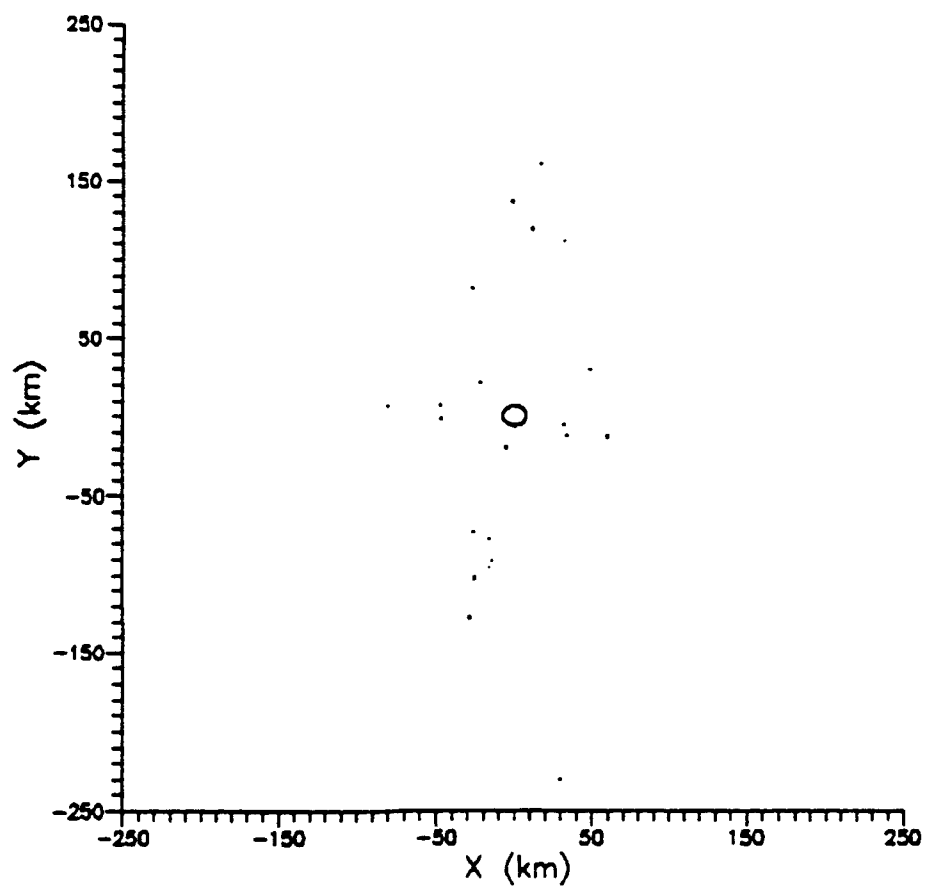
Figure 26. Surface of Section Plot for Orbit (-48,0)

73

Figure 27. Trajectory Plot for Orbit (-56,0)

74

Figure 28. Surface of Section Plot for Orbit (-56,0)

75

Figure 29. Surface of Section Plot for Orbit (-75,0)

Figure 30. Surface of Section Plot for Orbit (-75,0)

77

Figure 31. Surface of Section Plot for Orbit (-109,0)

7 8
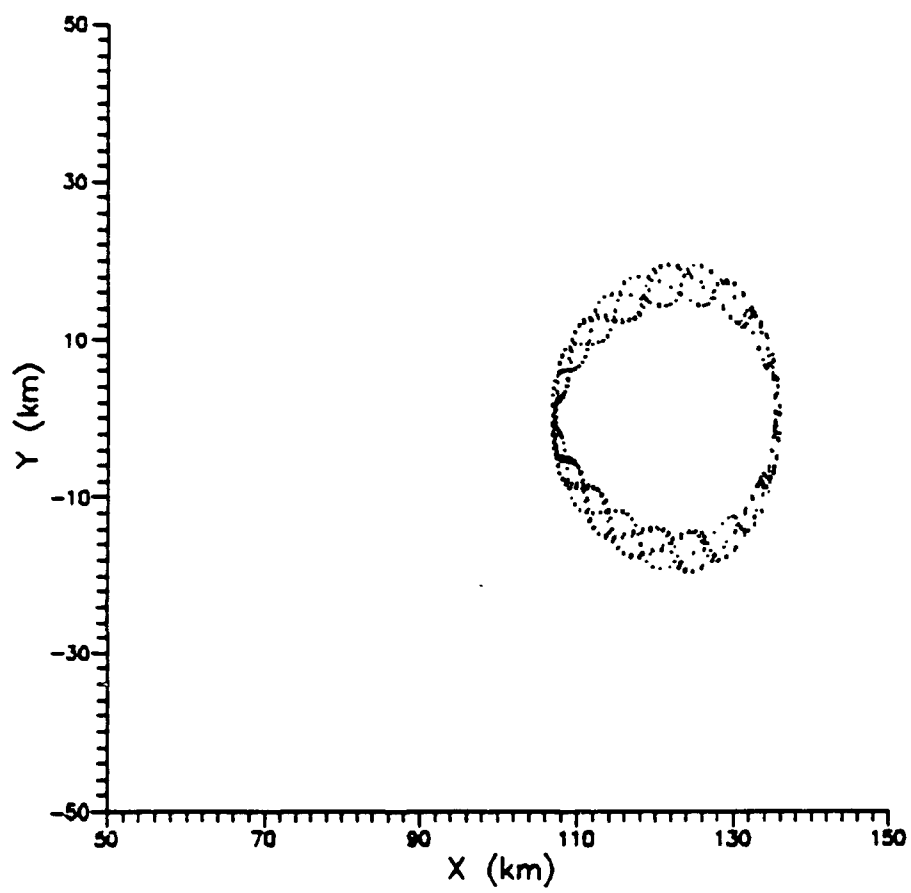
Figure 32. Surface of Section Plot for Orbit (-109,0)
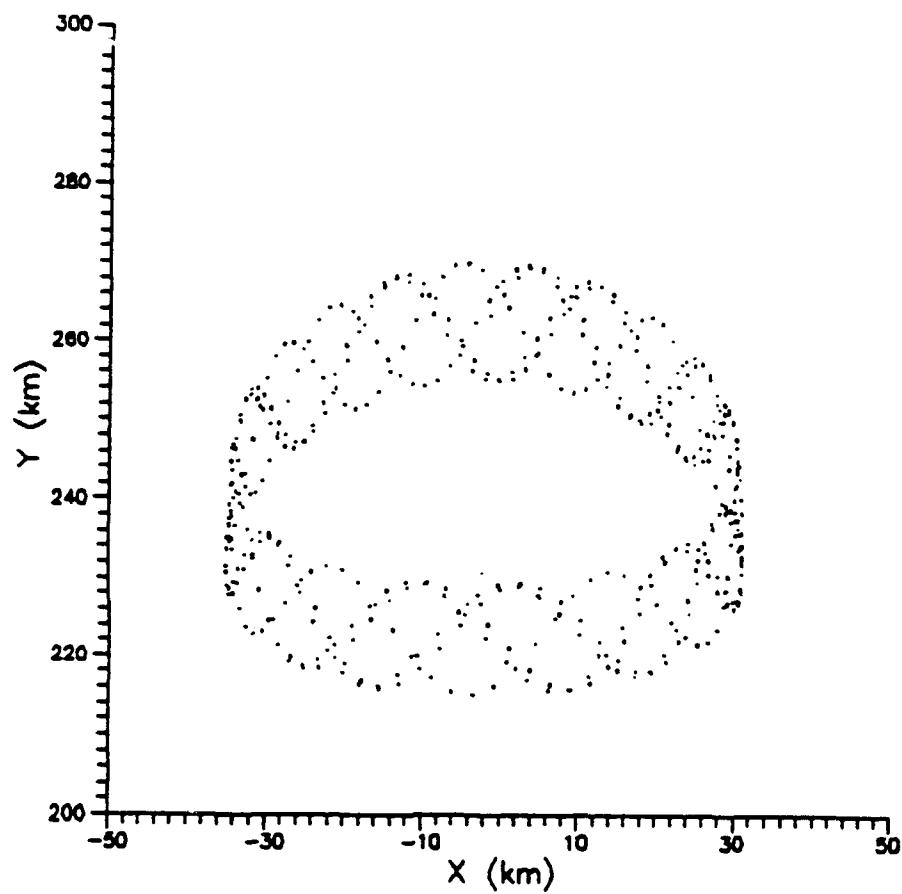
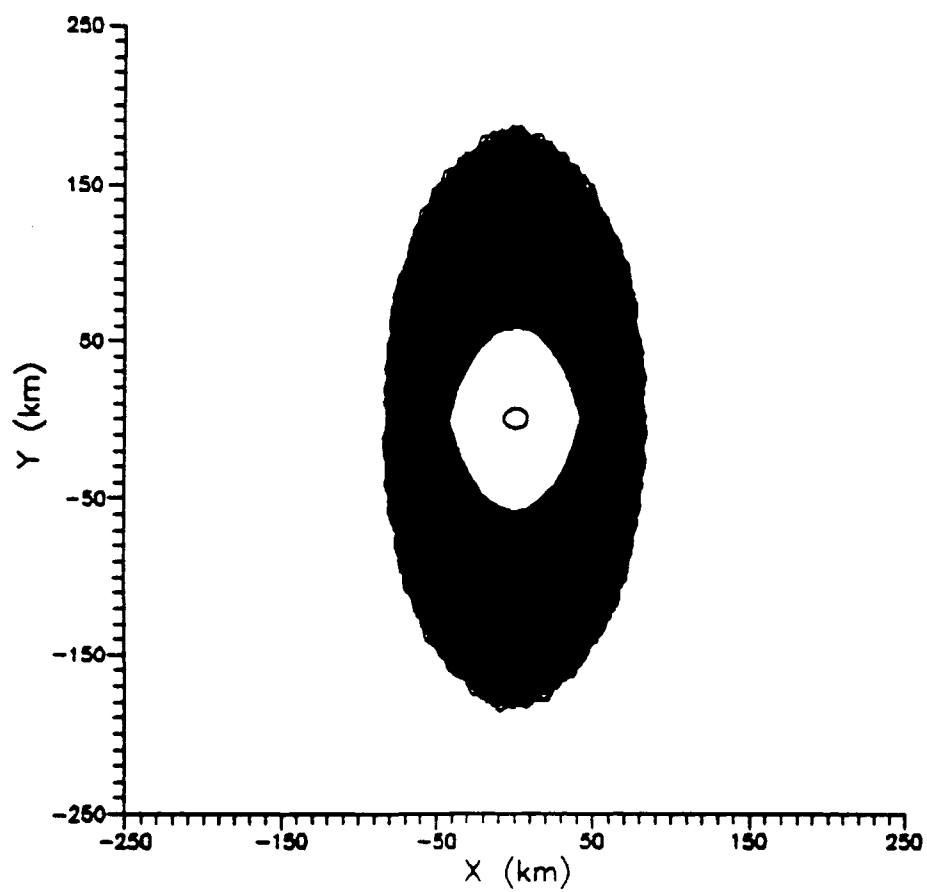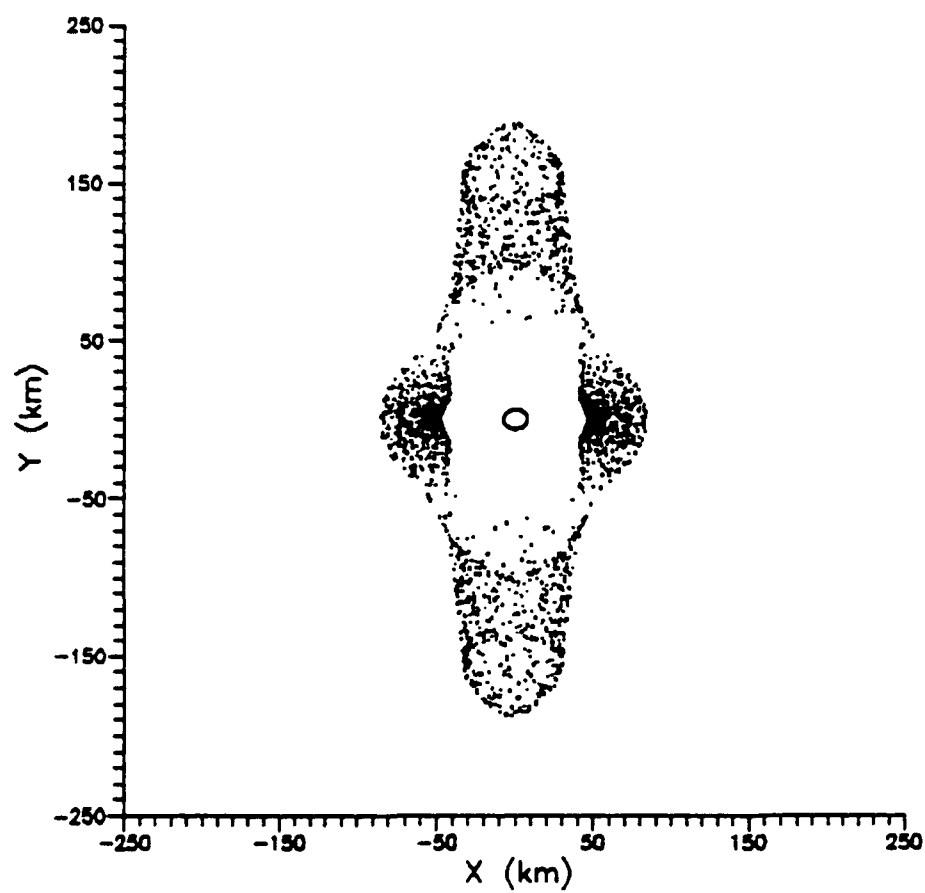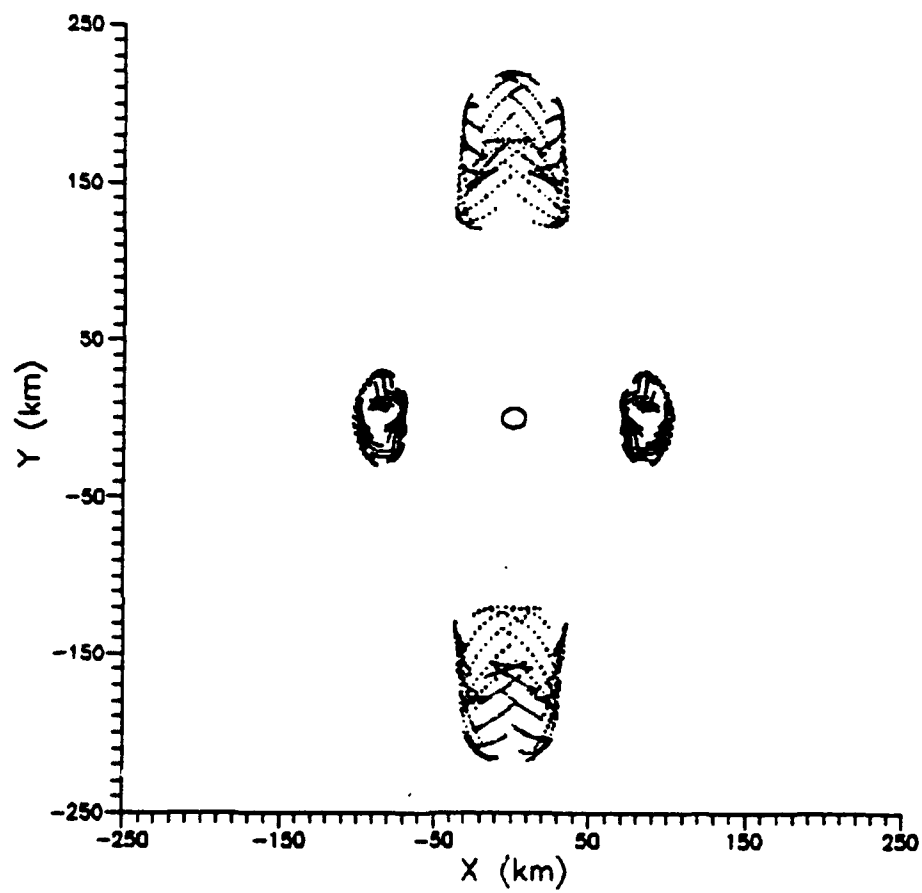Figure 33. Surface of Section Plot for Orbit (-109,0)
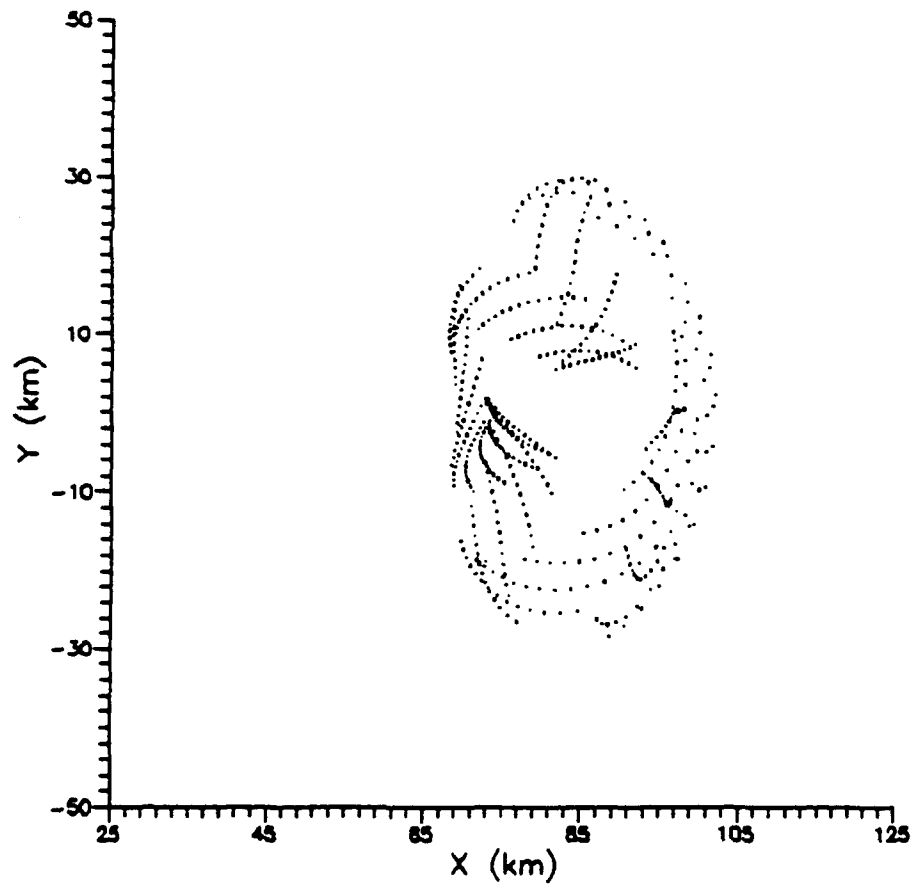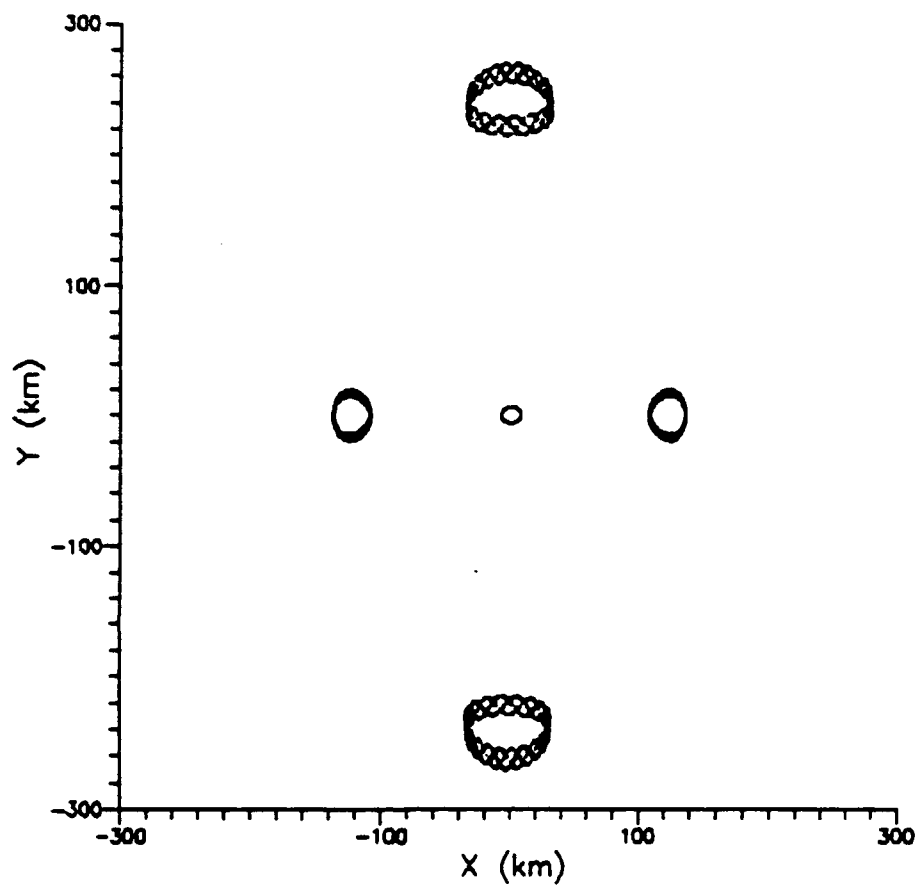
80
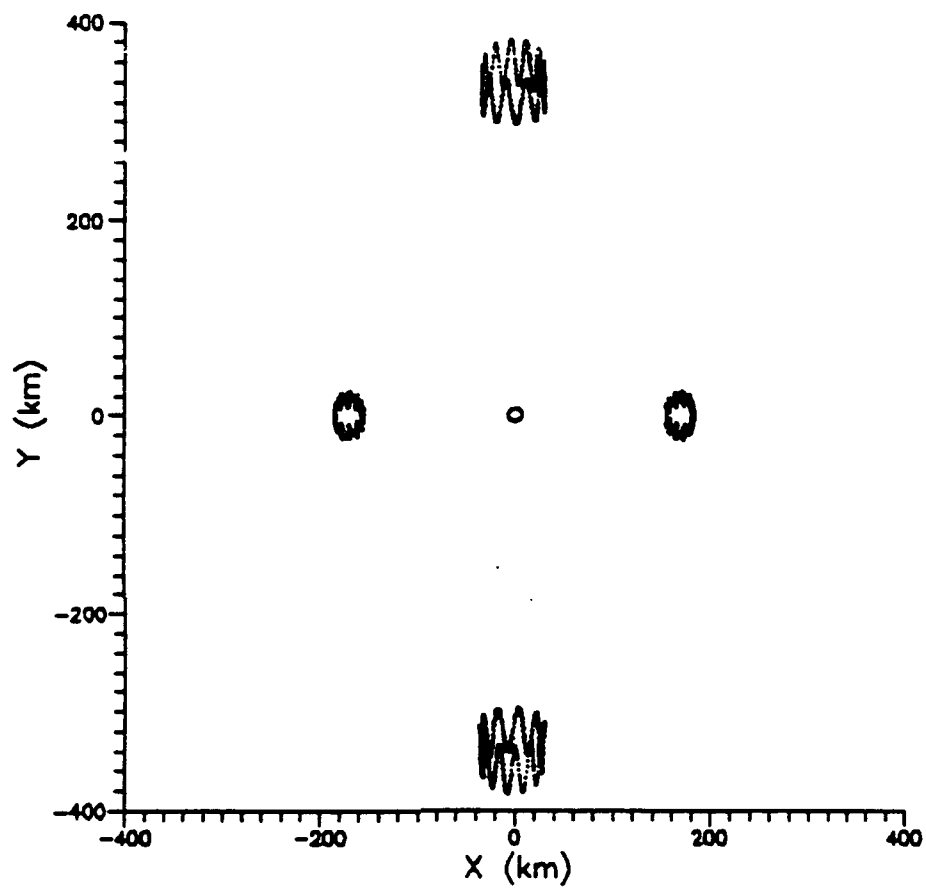
Figure 35. Surface of Section Plot for Orbit (-156,0)
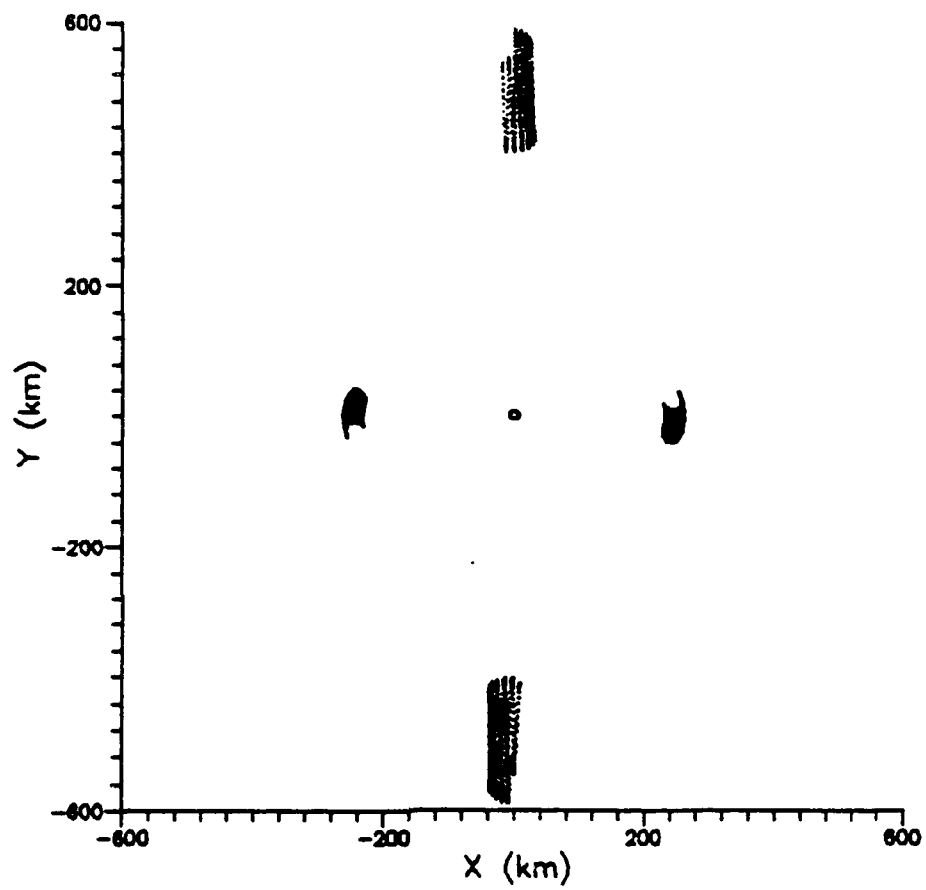
Figure 36. Surface of Section Plot for Orbit (-233,0)

83
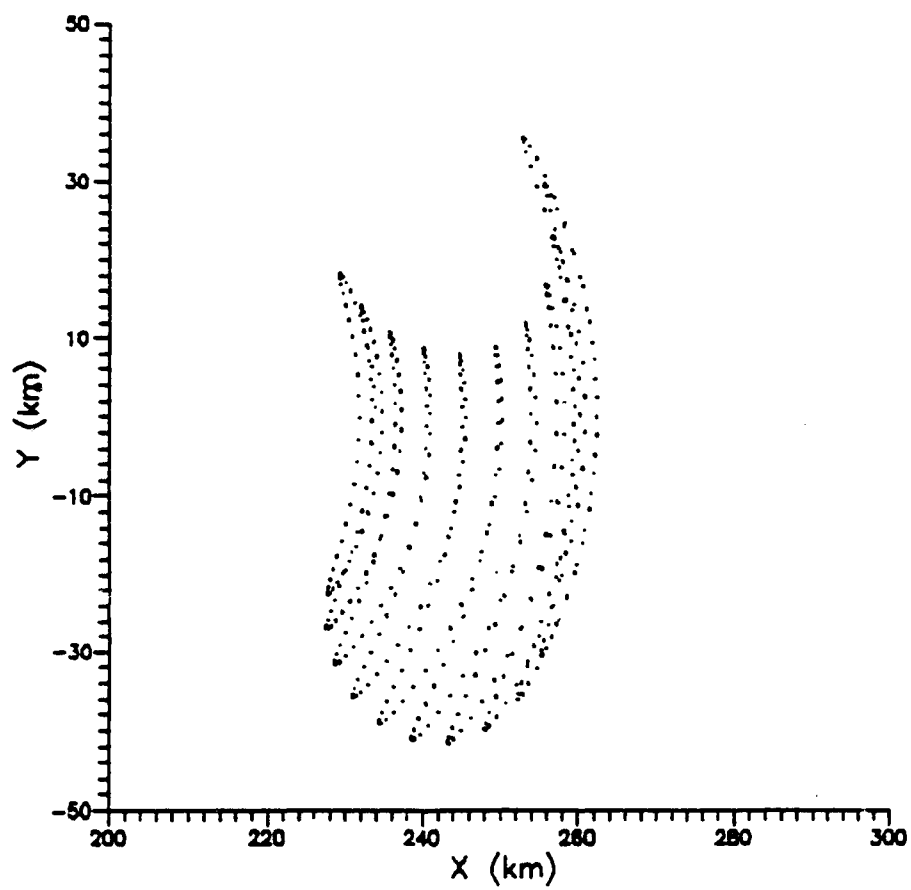
Figure 37. Surface of Section Plot for Orbit (-233,0)

Bibliography

1. Croswell, K. "Target: Phobos," <u>Ad Astra,1</u>: 17-21 (January 1989).

2. Lerner, E. J. "Phobos: Gains from a Loss," <u>Aerospace America,28</u>: 42-46 (February 1990).

3. Goldman, S. "The Legacy of Phobos 2," <u>Sky and Telescope</u>, 156-159 (February 1990).

4. Jansson, Capt S. W. <u>Stable Orbits about the Martian Moons</u>. MS Thesis AFIT/GA/ENY/89D-3. School of Engineering, Air Force Institute of Technology (AU), Wright-Patterson AFB OH, December 1989.

5. Brouwer, D. and G. Clemence. <u>Methods of Celestrial Mechanics</u>. New York: Academic Press, 1961.

6. Meirovitch, L. <u>Methods of Analytical Dynamics</u>. New York: McGraw-Hill Book Company, 1970.

7. Likens, P. W. <u>Elements of Engineering Mechanics</u>. New York: McGraw-Hill Book Company, 1973.

8. Wiesel, W. E. <u>Advanced Astrodynamics</u>. Class Lecture Notes for Mech 636, School of Engineering, Air Force Institute of Technology (AU), Wright-Patterson AFB, OH, December 1989.

9. Szebehely, Victor. <u>Theory of Orbits</u>. New York: Academic Press Inc., 1967.

10. Cheney, W. and D. Kincaid. <u>Numerical Mathematics and Computing</u>. (Second Edition). Monterey, CA.: Brooks/Cole Publishing Company, 1985.

11. Bates, R., D. Mueller and J. White. <u>Fundamentals of Astrodynamics</u>. New York: Dover Publications, Inc., 1971.

12. Smith, R. and G. West. <u>Space and Planetary Environment Criteria Guidelines for Use in Space Vehicle Development, 1982 Revision: Vol 1</u>. NASA Technical Memorandum 82478. Marshall Space Flight Center, Alabama, 1983.

Vita

Captain Samuel R. Bryant received the degree of Bachelor of Science in Aerospace Engineering from Mississippi State University in 1984 and was inducted into the National Honor Society for Aerospace Engineers. In 1985, he received his Air Force Commission as a distinguished graduate from Officer Training School in San Antonio, Texas. He was then assigned to HQ Space Division, Los Angeles AFB, CA., where he served as Mission Integration Manager for the Defense Satellite Communications System (DSCS) Phase III satellite program. During the next four years, Captain Bryant was responsible for coordinating all mission integration efforts for transporting, mating, testing, and launching the DSCS III satellite with its assigned launch vehicle which included the Titan 34-D, Titan IV, Space Shuttle, and the newly acquired Atlas II. He then entered the Graduate School of Engineering at the Air Force Institute of Technology in May 1989.

Captain Bryant is a member of Sigma Gamma Tau, AIAA, and the AFA.

Permanent Address: P.O. Box 55
                                  Port Barre, LA. 70577

REPORT DOCUMENTATION PAGE

1. AGENCY USE ONLY (Leave Blank)	2. REPORT DATE December 90	3. REPORT TYPE AND DATES COVERED Final

4. TITLE AND SUBTITLE Realistic Orbits About the Martian Moons	5. FUNDING NUMBERS

6. AUTHOR(S)

Samuel R. Bryant, Captain, USAF

7. PERFORMING ORGANIZATION NAME(S) AND ADDRESS(ES) School Of Engineering Air Force Institute of Technology	8. PERFORMING ORGANIZATION REPORT NUMBER AFIT/GA/ENY/90D-1

9. SPONSORING MONITORING AGENCY NAME(S) AND ADDRESS(ES)	10. SPONSORING MONITORING AGENCY REPORT NUMBER

11. SUPPLEMENTARY NOTES

12a. DISTRIBUTION AVAILABILITY STATEMENT	12b. DISTRIBUTION CODE

13. ABSTRACT (Maximum 200 words)

Orbits about the Martian moons, Phobos and Deimos, previously found to be stable by the Poincare surface of section technique in a restricted three-body system, were investigated with non-zero eccentricity of the moons added to the dynamics of the planar four-body system (Mars, moon, sun, artificial satellite). Although not strictly applicable to this case, the surface of section technique was used to verify whether or not the previously found stable orbits were realistic when a real world perturbation was added to the system dynamics. The surface of section technique involves the numerical integration of several orbits with the same initial value of the Hamiltonian based on matching the angular rates of the orbit and moon with respect to Mars. Apoapsis and periapsis points of the orbits were plotted in the two-dimensional configuration space. Stable orbits were found when the points formed regions which are bounded; chaotic orbits were indicated by random points.

14. SUBJECT TERMS Mars Phobos Deimos Poincare Surface of Section Orbits	15. NUMBER OF PAGES 99
	16. PRICE CODE

17. SECURITY CLASSIFICATION OF REPORT UNCLASSIFIED	18. SECURITY CLASSIFICATION OF THIS PAGE UNCLASSIFIED	19. SECURITY CLASSIFICATION OF ABSTRACT UNCLASSIFIED	20. LIMITATION OF ABSTRACT UNLIMITED